Doping / Functionalization and Characterization of Mono and Few Layer Graphene

By

Muhammad Asif

Supervisor Name: Dr. Habib Nasir

School of Chemical and Materials Engineering (SCME)

National University of Sciences and Technology (NUST)

2012

Doping / Functionalization and Characterization of Mono and Few layer Graphene

Name: **Muhammad Asif**

Reg. No: **2010-NUST-MS PhD-EM-E-06**

This work is submitted as a MS thesis in partial fulfillment of the requirement for the degree of
MS in Energetic Materials Engineering

Supervisor Name: Dr. Habib Nasir

School of Chemical and Materials Engineering (SCME)
National University of Sciences and Technology (NUST),
H-12 Islamabad, Pakistan

August 24, 2012

In the name of Allah

the Most Beneficent

the Most Merciful

Certificate

This is to certify that work in this thesis has been carried out by **Mr. Muhammad Asif** *(Reg. No: 2010-NUST-MS PhD-EM-E-06)* and completed under my supervision, in School of Chemical and Materials Engineering, National University of Sciences and Technology, H-12, Islamabad, Pakistan.

Supervisor: Prof. Dr. Habib Nasir _____

Co-supervisor: Dr. Amir Habib _____

Submitted through

Principal/Dean,

School of Chemical and Materials Engineering
National University of Sciences and Technology,
Islamabad, Pakistan

Abstract

Graphene has attracted much of interest of the researchers since it was successfully isolated for the first time due to its unique mechanical, electrical, optical and thermal properties. In current work, we have focused on doping and characterization of mono and few-layer graphene (MFLG) with methyl orange (MO) and Sudan IV. The study of thickness dependent doping effect is carried out by modifying MFLG sheets with MO molecules. Importantly, Surface-enhanced Raman Scattering (SERS) identification of trace quantity Sudan IV molecules is performed by using graphene as SERS substrate for the first time. The Sudan Red dyes can cause cancer in human body if taken in large quantity and are strictly forbidden by the "International Agency for Research on Cancer". This method can be used as economical and convenient method for detection of Sudan IV molecules and other such strictly forbidden colorants for the prevention of their usage in Food Colorants, Cosmetics and Disinfectants. The numbers of graphene layers are identified by optical microscopy, AFM and Raman Spectroscopy on oxidized silicon substrate. The optical microscopic identification based on color contrast between and oxidized silicon surface give a rough idea about the number of layers in graphene sheets but AFM measurement by step height of scanning line gave better confirmation. However, Raman Spectroscopy gives true identification of graphene layers. The surface morphology of FLG was analyzed by AFM, SEM and STM. The doping effect and induced band gap is characterized by Raman spectroscopy and UV/Vis Spectroscopy respectively. The Raman spectroscopy analysis of doped graphene shows that doping effect is thickness dependent and it is strong in mono layer graphene but decreases as the number of graphene layers increases. The UV/Vis spectroscopy analysis shows a 0.40eV increase in band gap of MO doped graphene. Furthermore, doping effect and increase in band gap are concentration dependent as well.

Dedication

Dedicated to My Respected Parents Mr. & Mrs. M. Afzal, Brother M. Rashad,
Caring Sisters Sumara & Tayyabah Afzal,
My Loving Mrs. Dr. Yasmin Asif and Beloved Daughter Noor-Ul-Wara Asif.

Acknowledgements

First and foremost, I would like to thank my advisor, Prof. Dr. Habib Nasir for giving me with generous guidance, expert advice through all stages of this research and other wide ranging research projects. I am also indebted to Dr. Sohail Ahmad Janjua (PINSTECH), Dr. Waheed Ahmad (UET-Lahore) and Dr. Amir Habib for sharing their knowledge for all equipment used in their laboratories. Without their assistance, the experiments presented in this thesis would not have been realized. I would also like to thank Prof. Dr. Iram Mehmood and Dr. Noaman Ul Haq members of GEC for their valuable suggestions and kind criticism.

I wish to acknowledge Prof. Dr. Habib Nasir for supporting my research project by providing extra funds for importing chemicals and materials. I would also thank to Prof. Dr. Lujun Pan and his student Dawei Li (Dalian University of Technology, China) for providing me excess to their laboratory for the improvement of some part of this research.

Finally, I would like to thank my parents, brother, sisters, friends and especially my wife for giving me support and encouragement throughout my postgraduate studies. Their love and companionship have been an essential source of strength to me during the course.

TABLE OF CONTENTS

List of Figures

List of Tables

List of Abbreviations

FLG	Few-Layer Graphene
MFLG	Mono and Few Layer Graphene
AFM	Atomic Force Microscopy
SEM	Scanning Electron Microscopy
TEM	Tunneling Electron Microscopy
STM	Scanning Tunneling Microscopy
SERS	Surface-Enhanced Raman Scattering
HOPG	Highly Oriented Pyrolytic Graphite
MO	Methyl Orange
PMMA	Poly Methyl Methacrylate
FWHM	Full Width at Half Maximum

Chapter 1 INTRODUCTION

1.1: INTRODUCTION

Carbon belongs to the forth group of the periodic table and is short lived but most stable in different multi-atomic forms. It is found in various molecular configurations that are known as allotropes. Carbon has three allotropes named as 1) - amorphous carbon 2) - graphite 3) - diamond. Graphite is thermally most stable and is chemically inert in ambient conditions. High temperature is needed for their reaction even with oxygen. All these allotropes exist in solid state under normal conditions.

Carbon was reported many years ago with different allotropic forms and research has been performed to explore the unique properties of carbon materials that can exist in different forms, 0-D(fullerenes), 1-D (nanotubes), 2-D (graphene) and 3-D (diamond & graphite), as shown in Fig 1.1.

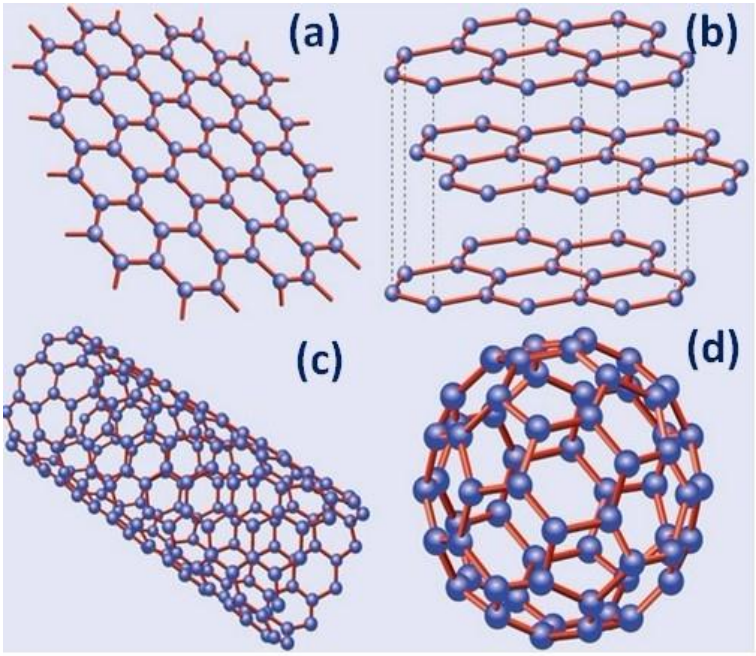

Fig 1.1: Different forms of carbon materials, 0D-fullerenes (d), 1D-nanotubes (c), 2D-graphene (a), and 3D-diamond & graphite (b) [1].

Graphene, the allotrope of carbon is a planer single layer of sp^2 hybridized carbon atoms arranged in the form of honeycomb two-dimensional (2D) lattice. The carbon to carbon bond length is of 0.142 nm [2]. Graphene can be stacked in multiple layers to form graphite.

If we discuss the electrical properties, electron's mobility in the graphene is very high such that they act as relativistic particles having zero mass, due to which graphene show quantum Hall effect and delocalization[3, 4]. Among the various exciting properties of graphene, first is high electron's mobility (250,000 cm^2/Vs) [5, 6]， second outstanding thermal conduction (5000$Wm^{-1}K^{-1}$) [7] and having Young's modulus of 1 TPa [8]. Graphene is widely used as gas detector, conducting electrode, composites and energy storage appliances i.e lithium ion batteries and super capacitors [8-21]. Induction of band gap leads graphene changes it to semiconducting material with a band gap ranging between 1 to 2 nm and have wide range of applications in transistors [9, 11]. Recently graphene is rising as prosperous material in scientific research for future electronic industry. Andre Geim and Konstantin Novoselov won the 2010 Noble Prize in physics "for ground breaking experiments regarding the two-dimensional material graphene'', a layer of graphite in the pencil.

1.2: PROPERTIES

Many important properties have been reported in past few years due to the rising interest level in exploring pristine graphene. Among its unique properties graphene shows high carrier mobility (230,000 cm^2/Vs) when absorption of visible light is 2.3% [22, 23], high thermal conduction (3000 W/mK), excellent mechanical strength of 130 GPa (modulus of elasticity 1 TPa), high specific surface area (2600 m^2/g) as well as half integer quantum Hall effect. This motivated scientific community to explore more of its properties. Some properties are discussed here.

1.2.1: Electrical Properties

Most of the experimental study on graphene stresses on the electronic properties. Before discussing the electrical properties of graphene it is better to know some information about its basics. In ground state carbon atom has four valence electrons. 2s subshell contains two and 2p subshell also contains two electrons. During the formation of bond with other carbon atoms via *sp* hybridization, one electron is shifted from 2*s* orbital to 2*p* orbital. There are three kinds of hybridization, i.e *sp* involving one s and one p orbital, sp^2 involving one s and two p orbitals and sp^3 involving one s and three p orbitals. In case of graphene, two *2p* orbitals hybridize with one 2*s* orbital to form three sp^2 hybrid orbitals which form sigma bonds with three neighbor carbon atoms in the lattice. Sigma bonds are very strong bonds so they contribute towards the mechanical properties of lattice but they do not

contribute towards the electrical properties. Besides electrons forming σ-bonds, there is another electron which occupies $2p_z$ orbital. Electrons in $2p_z$ of all carbon atoms overlap with neighbor to form *π-bond* which leads to electrical properties of graphene plane.

Graphene is very unique material in which charge carriers act as massless particles. These massless particles are known as Dirac fermions. Dirac fermions are different from those of electrons i.e in the existence of magnetic field they show integer quantum Hall effect also at room temperature [4, 24, 25] for both electrons and holes.

Because of its unique band structure, the graphene Quantum Hall Effect exhibits a subtle difference from the conventional Quantum Hall Effect in that plateaus appear at half integers of $4e^2/h$ rather than the distinctive $4e^2/h$.

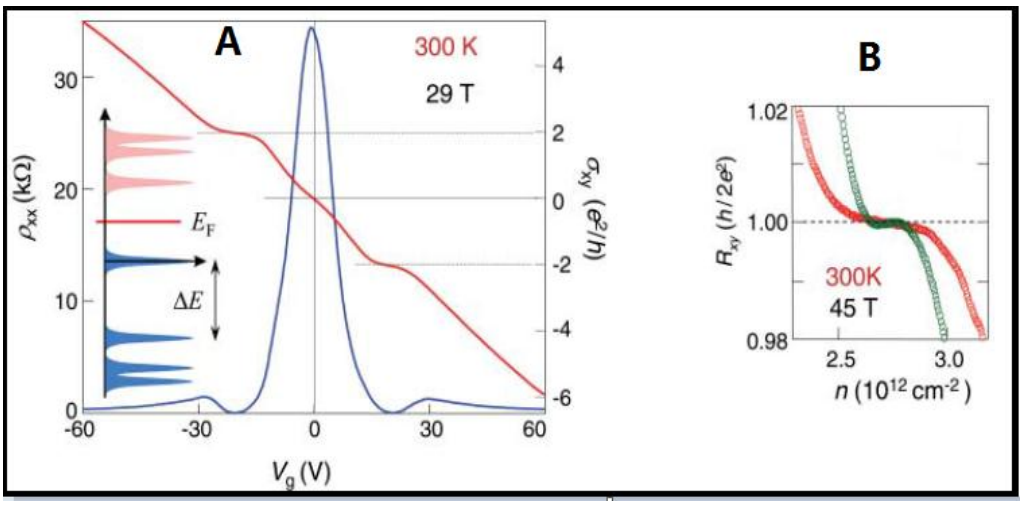

Fig 1.2: Room-temperature QHE in graphene. (A) σ_{xy} (red) and ρ_{xx}(blue) as a function of gate voltages (V_g) in a magnetic field of 29 T. Positive values of V_g induce electrons, and negative values of V_g induce holes, in concentrations $n = (7.2 \times 10^{10}\ cm^{-2}V^{-1})V_g$. (Inset) The Landau level (LL) quantization for Dirac fermions. (B) Hall resistance, R_{xy}, for electrons (red) and holes (green) shows the accuracy of the observed quantization at 45 T. Ref [4]

The band structure of single layer graphene shows that it consists of two bands. In reciprocal space these bands are at equivalent point K and K'. K and K' are known are Dirac points. At these points valance and conduction bands are degenerated which lead the graphene to be a zero band gap semiconductor. We can generate the

gap by applying electric field normal to plan of paper (Fig 1.3c). Details are shown in Fig 1.3.

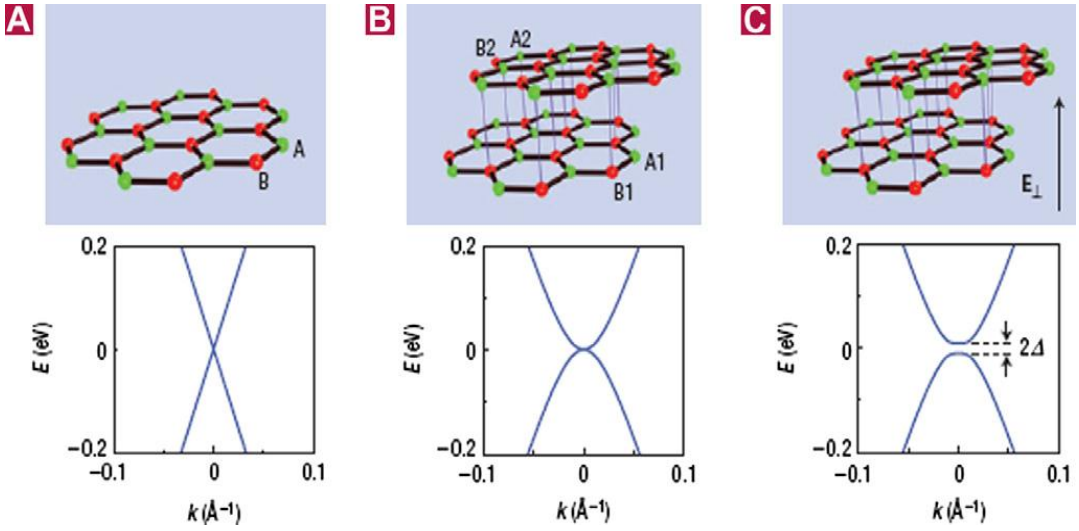

Fig 1.3: Band gap in graphene. Schematic diagrams of the lattice structure of (A) monolayer, (B) bilayer graphene and Insertion of band gap by electric field perpendicular to the bilayer graphene (C) [26].

Fig 1.3 shows band gap in graphene. Schematic diagrams of the lattice structure of (A) monolayer and (B) bilayer graphene. The green and red colored lattice sites indicate the A (A1/A2) and B (B1/B2) atoms of monolayer (bilayer) graphene, respectively. The diagrams represent the calculated energy dispersion relations in the low-energy regime, and show that monolayer and bilayer graphenes are zero-gap semiconductors. (C) When an electric field (E) is applied perpendicular to the bilayer, a band gap is induced in bilayer graphene, whose size (2Δ) is tunable by the electric field [26].

1.2.2: Optical properties

Light absorbance of single layer graphene was found to be 2.3% in many experiments over broad range of wavelengths as shown in Fig. 1.4 [23, 27]. Fine structure constant is very helpful to describe and explain the remittance of graphene [23, 28]. It is found that as number of layers increases absorption of light increases linearly. Here each layer absorption is given as $\mathbf{A=1-T=\pi\alpha=2.3\%}$ (where $\boldsymbol{\alpha \approx 1/137}$ is the fine structure constant). Graphene on the oxidized silicon substrate produces very fine color contrast due to Interference of light between graphene and oxide layers, which gives optical images of graphene. However, as the number of graphene layers increases the contrast of optical images increases which give identification of

number of graphene layers. Monolayer graphene absorption is uniform from 300 to 250 nm, while peak at 250 nm in Ultra Violet region is recognized to the transition in the electronic band from the empty π-states as shown in Fig. 1.4 [28].

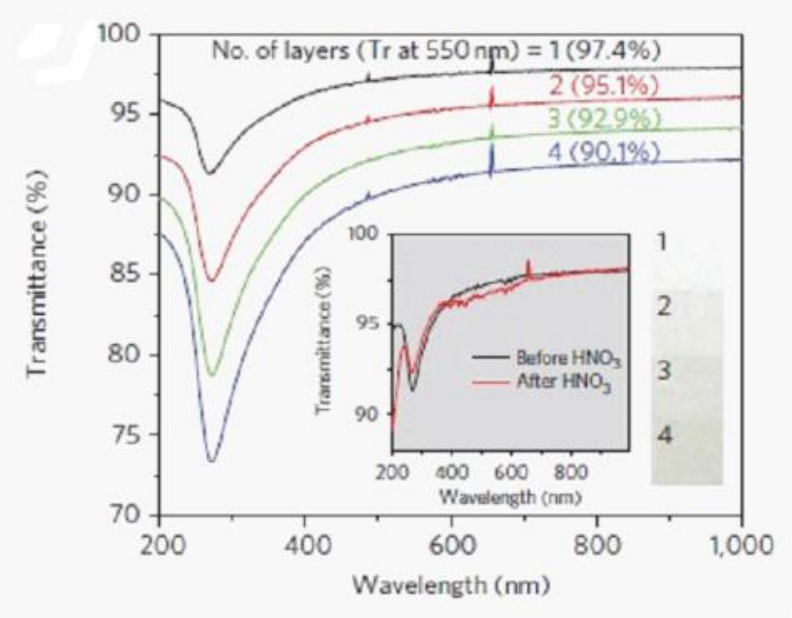

Fig. 1.4: Transmittance of different graphene layers. UV/Vis spectra of roll-to-roll layer-by-layer transferred graphene films on quartz substrates. The inset shows the UV spectra of graphene films with and without HNO_3 doping. The right inset shows optical images for the corresponding number of transferred layers ($1\times1cm^2$) [27].

Photo luminescence (PL) is another property of graphene in which suitable band gap is introduced in order to make graphene luminescent. There are two methods used for this purpose. In first method we cut the graphene into Nano-Ribbons (NRs) and quantum dots. While in second method we give physical or chemical dealing using different gases which leads in reduction of π electron conductivity [29-31]. As an example it was shown that PL can be initiated when single layer graphene is treated with oxygen plasma [32]. In this way top layer is etched to make hybrid structure (keeping the underlying layer unchanged). In case of liquid and solid GO PL is detectable but abundant chemical reduction leads to reduced PL of GO. On the other hand disorder of π network is due to oxidation and lead to opening of band gap[33].
In photonics and optoelectronics graphene has opened new avenues by combining its optical and electrical properties. There are many fields, in which graphene is used as potential material. Important applications of graphene are photo detectors, touch

screens, photo voltaic, LED, terahertz devices, optical limiters and transparent conductors.

1.2.3: Mechanical Properties

The performance as well as life of electronic devices can be affected by unwanted strain. When an external stress is applied then crystal material can alter atomic distances which may lead to re-arrangement in confined electronics charge. This might result in creation of band gap in the electronic structure as well as changes the electronic transport properties. Graphene is found to have high modulus of elasticity and strength beside the carbon nanotubes. Many scientists have investigated the mono, bi, and multiple graphene layers for their mechanical applications which are shortlisted in the Table 1.

Table 1: Mechanical properties of graphene

Method	Material	Mechanical properties	References
AFM	Single layer graphene	E=1±0.1 TPa σ_{int}=130±10 GPa at ε_{int}=0.25	[8]
Raman	Graphene	Strain~1.3% in tension Strain~ 0.7% in compression	[34]
AFM	Mono, bi, tri-layer graphene	E=1.02 TPa ; σ=130GPa E=1.04 TPa ; σ=126GPa E=0.98 TPa ; σ=101GPa	[35]

It is found that intrinsic tensile strength of a single, defect free layer of graphene is greater and hardness is same as that of graphite. Intrinsic mechanical properties of graphene can be studied by application of compression and tensile stress [36-38]. For monitoring phonon frequency in the presence of uniaxial tensile and hydrostatic stresses [39] Raman spectroscopy is very effective technique. It was found that tensile stress decreases the vibrational frequency mode so soften the phonons. On the other hand compressive stress increases the vibrational frequency mode so leads to the phonon toughening. Thus the study of strain functioned phonon frequency vibration gives the valuable data on stress transmission to individual bonds (for

suspended graphene) as well as interaction at atomic level of graphene to the underlying substrate (for supported graphene).

Raman spectroscopy is used to estimate tensile strain and compression of graphene layers. This can be done when variation in the G and 2D band with applied stress, is monitored. Splitting of G band occurs when strain is increased and leads to the red shift. Whereas at small strain i.e. 0.8%, 2D band gives red shift but without splitting [40]. Ni et al. [37] investigated the blue shift in Raman spectra for micromechanically exfoliated graphene and epitaxial graphene on SiC. They found that blue shift is due to compression in the obtained graphene. It was also found that electronic band structure can be changed with strain, so controlling strain can tune the band gap.

Freshly uniaxial strains can be carried by tuning the band gap [39]. In this procedure graphene layer is placed on flexible polyethylene terephthalate (PET). Then by expanding the PET in one direction uniaxial tensile strain up to approximately 0.8% is applied on mono to tri layer graphene which gave band gap of 0.25 eV for single graphene layer. It was also suggested that uniaxial strain leads to breakdown of bond of C-C lattice which overstate the electronic properties of graphene much more dramatically.

1.2.4: Thermal Properties

Low carrier density of un-doped graphene leads to the negligible thermal conductivity (Wiedemann-Franz law). The thermal conductivity (***k***) of graphene depends on phonon transport. At high temperature diffusive conduction and at suitably low temperature ballistic conduction occurs [41]. Molecular Dynamics (MD) simulations [42] grounded on the Green-Kubo methodology showed a $k \propto 1/T$. It was found that thermal conductivity of a suspended monolayer graphene is about 6000 Wm^{-1} K^{-1} which was higher than that of graphitic carbon [42]. When Boltzmann equation based calculations were done then it was found that ***k*** depends on the width ***d*** of Graphene Nano Ribens (GNRs) and on the roughness of the edges, where the diffusive conduction governs ***k*** [43]. Investigation of the ***k*** of GNRs was done by using Non-equilibrium MD with different edge shapes as a function of strain, length and width [44]. If L is length of GNRs and β ranges from 0.3 to 0.5 at room temperature then it was found that $k \propto L^{\beta}$. Thermal conductivity depends on length of GNRs, so there is a long phonon mean free path in GNRs.

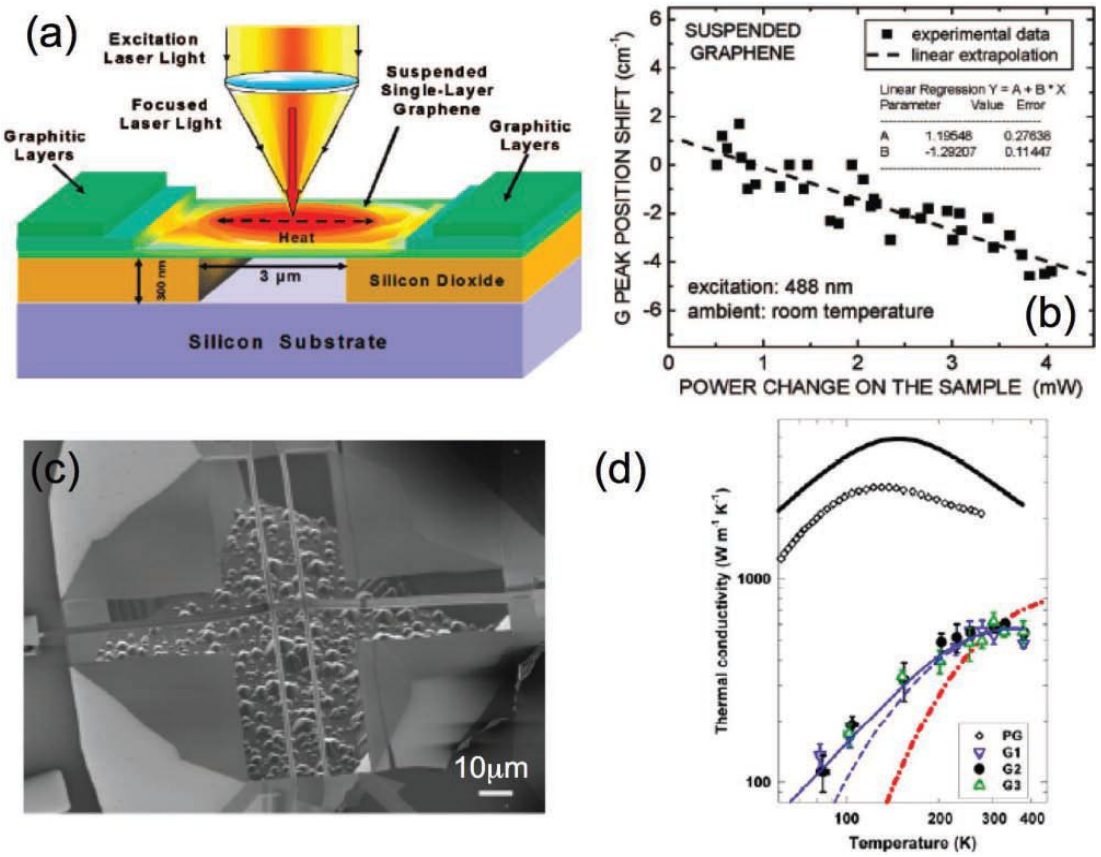

Fig. 1.5: (a) Schematic diagram of an experiment showing the excitation laser light focused on a graphene flake suspended across a trench. The focused laser light creates a local hot spot and generates a heat wave inside graphene propagating toward heat sinks; (b) Shift in Raman G peak position versus change in total dissipated power. The sample was excited at 488 nm and spectra were recorded at room temperature in the backscattering configuration. (c) SEM image of the suspended device for the thermal conductivity measurement of graphene. (d) Measured thermal conductivity values of graphene devices G1, G2, and G3, the highest reported values of pyrolytic graphite (PG), along with the Boltzmann transport equation (BTE) calculation results of suspended graphene (thick black solid line) and supported graphene (thin blue solid line and blue dashed line), as well as the relaxation time approximation (RTA) calculation result (thick red dash-dot line) for supported graphene. Specular edges are assumed in the calculations. Ref[45] for (a, b) and Ref [49] (c, d).

Recently for suspended and mechanically exfoliated monolayer graphene measurements using change in Raman G spectra, thermal conductivity of 5000 $Wm^{-1}K^{-1}$ was gained (Fig 1.5a) [45, 46]. In Fig. 1.5 when laser beam is concentrated on

the center of suspended graphene then heat flows towards supports. During heat flow heat loss in the air is very small as compared to the heat conducting in the graphene [47]. When temperature of graphene increases then heat results in softening of bonds. Therefore G peak shows red shift. In case of low laser power, red-shift of G band of graphene depends linearly on the temperature of the sample [48]. In Fig. 1.5 (b) G peak frequency was calculated as function of excitation power from the slope of the trend line (where thermal conductivity is 5000 $Wm^{-1}K^{-1}$). Recently it was found that thermal conductivity (about $600Wm^{-1}K^{-1}$) of micromechanically exfoliated graphene on silicon dioxide substrate exceeds than metals like Cu (Fig. 1.5 c, d) [49]. This value of thermal conductivity was lower than found for suspended graphene, whether micromechanically exfoliated [45] or CVD grown [50]. It was attributed to the leakage of phonons across the graphene-support interface and strong interface scattering of flexural modes [49].

1.3: SYNTHESIS ROOTS

There are various methods and techniques to synthesize graphene. Here we will discuss some important techniques to produce high quality graphene.

1.3.1: Mechanical Exfoliation

Bulk graphite consists of millions of graphene layers stacked in an ordered way. Vander Waals interactions are present between the graphene layers to hold them into a compact form. These interactions are so weak that interaction energy of $2eV/nm^2$ is present between the layers and force having magnitude 300 $nN/\mu m^2$ is needed to separate the layers of graphite [51]. Adhesive tape can be used to obtain this small force. In this top–down approach, Novoselov and Geim developed an effective method using adhesive tape. Adhesive tape was stuck and peeled several times and it gave 1 µm thick graphite fragment to a monolayer thin sample. Smoothness and thickness of graphene was investigated using AFM and later on exfoliated pieces were pressed to shift them onto cleaned substrate [25]. The characteristic of experiments lies in the selection of substrate. For human eye visualization, apparent contrast of monolayer graphene on Si/SiO_2 substrate (where oxidized layer is 300 or 90 nm) is definitely zoomed upto 12% at 550 nm, as shown in Fig. 1.6.

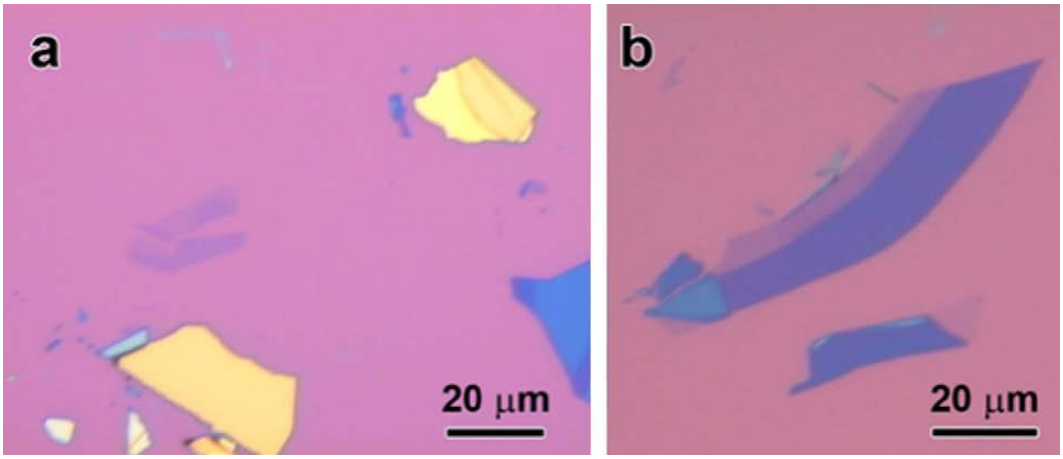

Fig. 1.6: Optical images of micromechanically exfoliated thin graphite & few-layer graphene (FLG) (a) and single-layer graphene (lighter purple contrast) on a ~300 nm SiO_2 layer (b). Yellow-like color indicates thicker samples (~ 100 s of nm) while bluish and lighter contrast indicates thinner samples.

On a 300nm oxidized silicon wafer, the graphite flakes which are thick appear yellow. However, as the thickness of flakes decreases, their color changes from yellow to blue as shown in Fig. 1.6 (a). The Fig. 1.6 (b) shows when thickness of graphene flakes reaches to sub-10nm then dark to light shades of purple color appear which illustrate single and few layer graphene. As interference phenomenon in the substrate is responsible for graphene visibility so with preserved reflectivity one can change at will by adjusting the thickness of dielectric layer. This technique has one disadvantage. The carrier mobility can be limited as it leaves residues stuck on the sample which is the only disadvantage of this technique [52, 53]. In order to avoid this disadvantage normally two methods are used; first method involves boiling at 200^{o}C for one hour in the presence of hydrogen/argon [54] and second method involves joule heating up to approximately 500^{o}C under vacuum [55].

As micromechanical exfoliation starts from single graphite source which is crystalline, so graphene produced by this method is of high quality and high electrical conductivity. Therefore Micromechanical exfoliation is the best method. However using this method one can't produce large area graphene. This method is good only for producing small size graphene. This reason inspired the scientist to find other methods for production of graphene.

1.3.2: Sublimation of Silicon carbide

In this method silicon carbide is annealed through ultrahigh vacuum (UHV) for manufacturing of graphite. In this way product is obtained on the SiC substrate so for

processing devices have no need of transfer process. This easiness makes it attractive approach in semiconductor industry [56-58]. Silicon carbide is heated in the presence of ultrahigh vacuum, as silicon atoms sublimates from the surface of substrate, remaining carbon atoms rearrange to form the layer known as graphene. The thickness of graphene layer depends upon two factors, first is temperature and second one is annealing time, by controlling these two factors we can control the thickness of graphene.

Few layer graphene can also be produced at approximately 1200^{o} C when SiC is annealed for few minutes [59]. Freshly FLG on SiC is produced by using vapor phase annealing. This method can form FLG of homogenous thickness, when 400^{o}C temperature above UHV is used [60, 61]. The application of this method is difficult because different SiC polar faces (i.e. Si-face or C-face) are used for different epitaxial growth; also it was observed that multilayer graphene on C-face surface gives unusual rotational stacking to graphene, but it is absent in case of Si-face surface. Such complications are big hurdle for production of graphene on commercial scale; therefore researchers explored another method for production of graphene which is known as chemical vapor deposition method.

1.3.3: Chemical Vapor Deposition

During the research on methods for production of carbon nanotubes on commercial scale, some investigation is also done on the decay of hydrocarbons into graphitic materials [62, 63]. We know that surface of a metal is very effective to catalyze such conversion. Chemical vapor deposition (CVD) is another way which enhances the growth of graphene on metal surface [64]. Now a days this technique is used to produce and investigate the characteristics of few to multi-layer graphene [65-67]. In 2011 many scientist used this method to prepare single and multilayer graphene by using altered metal catalyst and hydrocarbon source.

Investigation on high quality mono and bilayer graphene was done by Wei et al. [68]. During investigation they used copper as substrate and methane gas as source of hydrocarbon, they concluded that for the growth of graphene quality and pretreatment to copper substrate plays important role besides process parameters. Uniformity of grown graphene depends on micro topography of Cu surface, it was also concluded that at low pressure conditions purity of Cu plays important role in controlling the number of graphene layers. During the formation of graphene, hydrocarbon pressure should be Minimum for covering the Cu surface.

Madhav et al. [69] used copper substrate, methane and hydrogen gas mixture at the atmospheric pressure in CVD process to synthesize graphene, Later they used synthesized graphene to investigate the gas sensing properties. During the process films of graphene were shifted to different substrates when wet etching of copper substrates is finished. It was observed that gas concentration, gas nature, test temperature and gas composition are very important in order to characterize gas sensing properties i.e sensitivity, response and recovery time, sensitivity was also examined by using gasses such as NH_3, CH_4 and H_2.

Xuli et al. [70] also investigated CVD method. They used single crystal flake of hexagonal boron nitride to prepare few layer graphene (without using metal catalysts) and examined prepared graphene using Raman spectroscopy and TEM.

In 2009, Hye et al.[71] used CVD process to prepare few layer graphene by using Ni as metal substrate and methane as hydrocarbon. The prepared few-layer graphene was examined for it structural, optical, electrical and mechanical properties by using different instruments.

By CVD process metal substrate and hydrocarbon source involves in three steps for the formation of graphene layer. In the first step hydrocarbon breaks to form carbon atoms and in the second step carbon atoms adsorbed to surface of annealed metal to form nucleation center and in third and final step carbon atoms attached to their nucleation centre to from graphene layer. It has been found that number of graphene layer depends upon the concentration of carbon atoms, partial pressure of hydrocarbons, temperature and growth time. CVD is cheaper method as compared to mechanical exfoliation and epitaxial growth which are expensive and require high temperature. So recently majority of researchers are using this method to produce large area production of graphene for use in electronic industries.

1.3.4: Chemical exfoliation

Chemical exfoliation is an old technique for synthesis of graphene having high-yield and scalability. This method requires two steps, in first step graphite intercalated compound (GICs) is formed in order to increase spacing between sheets [72, 73]. There are many types of intercalants to produce GICs but not all of them are suitable for exfoliation process [73]. We can form GICs by using a very famous method in which graphite is soaked in mixture of nitric acid and sulfuric acid [74, 75]. In second step GICs are subjected to higher temperature, thermal annealing in ball milling and ultra-sonication increase the amount of exfoliation [75-77]. SLG sheets

can be obtained by repeating the intercalation and exfoliation process using different intercalants [78, 79]. Alternatively we can oxidize the graphite to form GOs [80, 81]. GOs can be exfoliated to form thin GO sheets using various methods [82].

In order to obtain SLG sheets, Horiuchi and coworkers have developed a process involving two steps and obtained what they called carbon Nano films [83, 84]. During the first step Hummer's method was used to oxidize graphite using sulfuric acid, $NaNO_3$ and $KMnO_4$ and obtained GICs (or GOs). In second step, the GOs were hydrolyzed to introduce the hydroxyl and ether groups into the inter graphene layer spaces. After this every GO layer becomes anion (multiply charged) and its thickness is about 0.6nm. During the purification process, when extra small ions from oxidants were removed, the GO sheets are disjointed. Obtained GO sheets when dispersed in water they form stable dispersion. In this way Horiuch et al. [83] succeeded in obtaining SLG sheets.

1.3.5: Un-zipping CNTs and Other Methods

Another method for production of graphene is by using Multi walled carbon nanotube (MWNT) and this process is called un-zipping of CNTs. It was found that one can intercalate lithium and ammonia in order to open the MWNTs in the along its length. Acids and sudden heat treatment is used to exfoliate the intercalated MWNTs [85] (Fig 1.7a), the resulting products contain graphene flakes, Nano ribbons and incompletely opened MWNTs. In plasma etching of MWNTs produces graphene nano ribbons which are partly fixed in a polymer film [86], MWNTs can be etched and change into graphene.

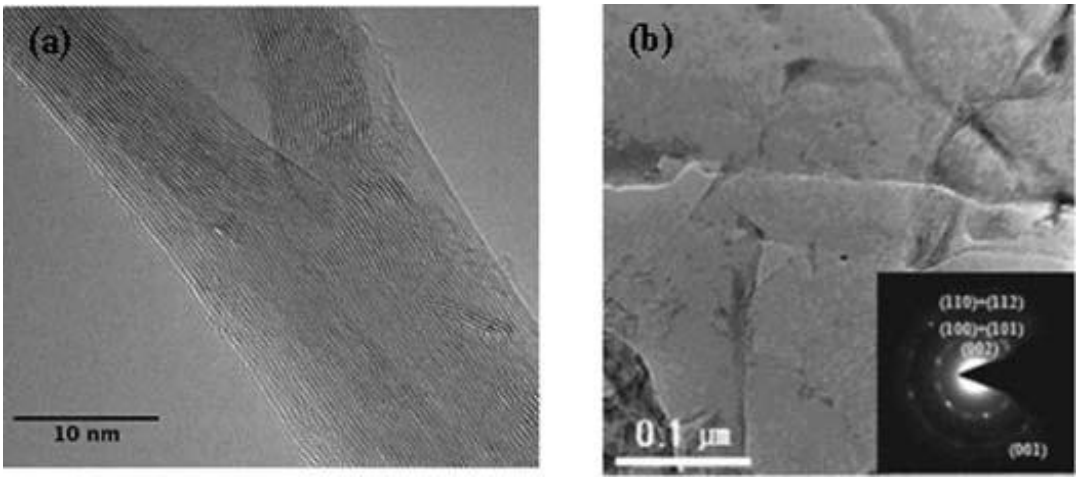

Fig. 1.7: (a) TEM image of partially unzipped MWCNT structure, opened by Li intercalation [85] and (b) high magnification TEM image of graphene sheet produced by multistep oxidation-reduction treatment. The inset is the SAED pattern, which confirms the crystalline nature of the graphene sheet.[87]

In some methods chemical treatment is used to unzip the MWNTs. Exfoliation is done by using concentrated sulfuric acid, $KMnO_4$ and H_2O_2. $KMnO_4$ is used for oxidization and reduction in NH_4OH and ($N_2H_4.H_2O$) solutions [88]. This new technique is free of substrate.

Recently multilayer graphene sheet was obtained when Al_2S_3 was calcined under gaseous environment of CO and Ar [87] (Fig 1.7b). In this technique first of all carbon mono oxide is reduced by Al_2S_3 to produce carbon gas and α-alumina, alumina particles are used to crystallize the graphene sheets. Although this process is very simple but its mechanism is not yet well understood. In future we can obtain bulk graphene on commercial scale but the necessity is to control of process parameters and number of graphene layers.

Micro-cantilever (for example an AFM tip) is also applied to produce graphene but thickness of product is 10-100 nm, which can't be treated as graphene. Highly oriented pyrolytic graphite (HOPG) was sliced using micro-cantilever in order to form graphene [89].

Chapter 2 DOPING OF GRAPHENE

2.1: DOPING OF GRAPHENE

Unique structure and properties of graphene lead the scientists to modify its electronic band structure by substituting the impurity atoms with carbon atoms, the process is known as doping of graphene. Doping of graphene is an interesting field; there are two types of doping methods. First type of doping includes gate-controlled doping [90, 91], doping with metallic cluster [92], substrate-induced doping [93] and is known as Electrical doping. The second type of doping includes the chemical methods i.e doping by substituting graphene lattice structures with heteroatoms [94] or molecules [95] , and is known as Chemical doping. In our current work, we will discuss only chemical doping of graphene.

Previously chemical doping of graphene was gained by surface adsorption and insertion of dopant atoms between the graphene layers. Work function of material plays important role in this respect. If work function of graphene and metals are different then charge can easily transfer between them [96]. Charge shifts towards material having greater work function. If work function of metals is higher than graphene then charge will migrate from graphene to the metals (p-doping). But if work function of metals is lower than that of graphene then charge will migrate from metal to graphene surface (n-doping). But in case of organic adsorbents, electron affinity or ionization energy of organic molecule and work function of graphene, difference is responsible for charge transfer between them. The charge migration changes the electrical atmosphere on the surface of graphene. For example induced positive electrical potential leads to the p-doping of graphene and in the same way negative electrical potential leads to the n-doping of graphene. We can also recognize the doping by observing the chemical enhancement of molecular Raman signals [97].

Chemical doping of graphene is done by chemical species, for example substitution atoms might be Nitrogen [94], Boron [98], Sulfur [99], and Si [100]. Adsorbed inorganic molecule e.g nitrogen dioxide [101, 102], nitric acid [103] as well as organic molecules e.g toluene [104] can also be used for chemical doping of graphene. In case of substitutional graphene doping, heteroatoms of dopant species replace the carbon atoms in hexagonal structure of graphene. This replacement

changes the sp^2 bonding of carbon atoms which leads to change of electronic band structure and properties. When Field Effect Transistors (FETs) are produced using graphene then some water or adsorbed oxygen is present on the surface of graphene. The presence of adsorbed oxygen or water leads to the p-type conduction in the FETs. On the other hand we also need n-type graphene FETs; it is solved by chemical doping. Theoretical investigation shows that if nitrogen atom is substituted in the plane of graphene then this N atom will adapt and modify the electronic properties of graphene and leads to n-type behavior which is very beneficial in the field of electronics [105]. It is reported that FETs using nitrogen doped graphene production [106, 107] is revealed using fresh experimental work. Synthesis techniques and electrical properties of nitrogen-doped graphene (NG) and pristine graphene (PG) are shown in table-2.

Table 2: Synthesis approaches as well as the electrical properties of nitrogen-doped graphene (NG) and pristine graphene (PG).

Sample	**Synthesis technique**	**No of Layers**	**Mobility (cm^2/Vs)**	**Reference**
NG sheets	CVD (CH_4+NH_3 as precursor, Cu film as substrate)	2-6	200-450	[106]
NG sheets	CVD (Pyridine vapor as precursor, Cu foils as substrate)	1	5	[107]
NG sheets	NH_3 annealing after N+-ion irradiation of mechanically exfoliated single-layer pristine graphene	1	6000	[108]
PG sheets	CVD (CH_4 as precursor, Ni film as substrate)	1-12	100-2000	[109]
PG sheets	CVD (CH_4 as precursor, Cu foil as substrate)	1-3	4050	[110]
PG sheets	Chemically reduced graphene oxide sheets	-	2-200	[111]

Carrier motility of NG sheets, which are synthesized by chemical vapor deposition [106, 107] is found to be less than that of PG sheets [109, 110]. The reason of low carrier mobility is that in case of NG, N atoms which are substituted in graphene lattice leads to extra scattering centers as compared to the PG sheet which is undoped. Chemical vapor deposition synthesis of NG sheets leads to introduction of defects which behave as scattering centers. Dopants and defects produce high scattering effect therefore become an obstacle in the transportation of electrons or holes. This decreases the carrier mobility of NG sheets but NG sheets which are obtained from the mechanical exfoliation of graphite [108] have high carrier mobility than the CVD-grown NG sheets [106, 107] and PG sheets [109, 111]. High crystal quality of starting graphite material leads to such a result. Theoretical investigation showed that heteroatoms for example sulfur [99], [112], phosphorus [99], boron [98, 113, 114] [9,25,26] and silicon can also be used for the doping of graphene and their prospective applications have been studied. Let us take the example of sulfur doped graphene (SG). Density functional theory (DFT) calculations showed that presence of NO_2 gas leads to its adsorption on the SG. Therefore density of states (DOS) of SG increases at Fermi point. This observation shows that SG is highly sensitive material for detection of toxic gases [99]. Also first-principle calculations revealed that different location and concentration of heteroatoms can be used to produce different transport effects during S-doping. On comparison with pristine graphene sheets [115], doped sheets show metallic behavior or as small band-gap semiconductor. So band gap of graphene can be tuned using chemical doping and gap variation is dependent on dopants concentrations and its locality in graphene.

Apart from substitutional doping, significant changes occur in electronic transport of carbon sheet which can be induced by physical adsorption of dopant molecules on the surface of graphene. Physical adsorption causes the shifting of charge between graphene and adsorbed dopant molecules, therefore adjust the carrier density in graphene. Control of Dirac point is very essential in the electronic applications. Effective offset voltage is produced by chemical doping of molecules. Offset voltage produces the extra displacement field in order to open that band gap and also changes the Fermi energy level. In this field, numerous inorganic and organic molecules have been examined as adsorbed dopants on the surface of graphene sheets. Inorganic molecules i.e NO_2 [101, 102] , HNO_3 [103] and organic molecules

i.e benzyl viologen [95] , toluene [104] , melamine [116] and triazine [117] have been used as adsorbed dopants. As we know that graphene can be regarded as zero band gap semiconductor. Therefore, when gate voltage is applied then electron and holes transportation is symmetrical but when graphene FETs is doped then it behaves as p-type due to presence of oxygen and water molecules which are adsorbed on graphene surface during its exposure to the air. Besides adsorption of organic molecules (containing nitrogen) on graphene surface leads to n-type behavior [95]. Depending upon above investigations, we can dope graphene FETs by placing different molecules on the graphene sheets, the Schematic design of a bi-layer graphene FET which is doped with benzyl viologen [95] is shown in Fig. 2.1(a). The Fig. 2.1(b) shows Electrical measurements of the switching characteristics. We can change electrical field held in perpendicular which tune the on/off ratio of devices having p and n-type behaviors [95]. Besides benzyl viologen and melamine can also be used for doping of graphene. If we look at Fig. 2.1(c) then we can find that melamine adsorption shifts the Dirac point towards positive gate voltages, this shows that electrons are migrated from graphene to the melamine. Carrier concentration up to 1.4×10^{13} cm^{-2} can be adjusted by controlling the melamine molecule concentration and temperature during the doping [116]. Earlier work revealed that on/off ratios of graphene-based FETs can be improved by n-type doping. The Fig. 2.1(d) shows the on/off current ratios, where the thermal annealing is done in the vacuum and triazine is used to decorate the bilayer graphene devices [117]. When N atoms are introduced in the ring of triazine, then triazine becomes rich in electrons. Therefore, electrons are shifted to the graphene surface, as result it behaves like n-type.

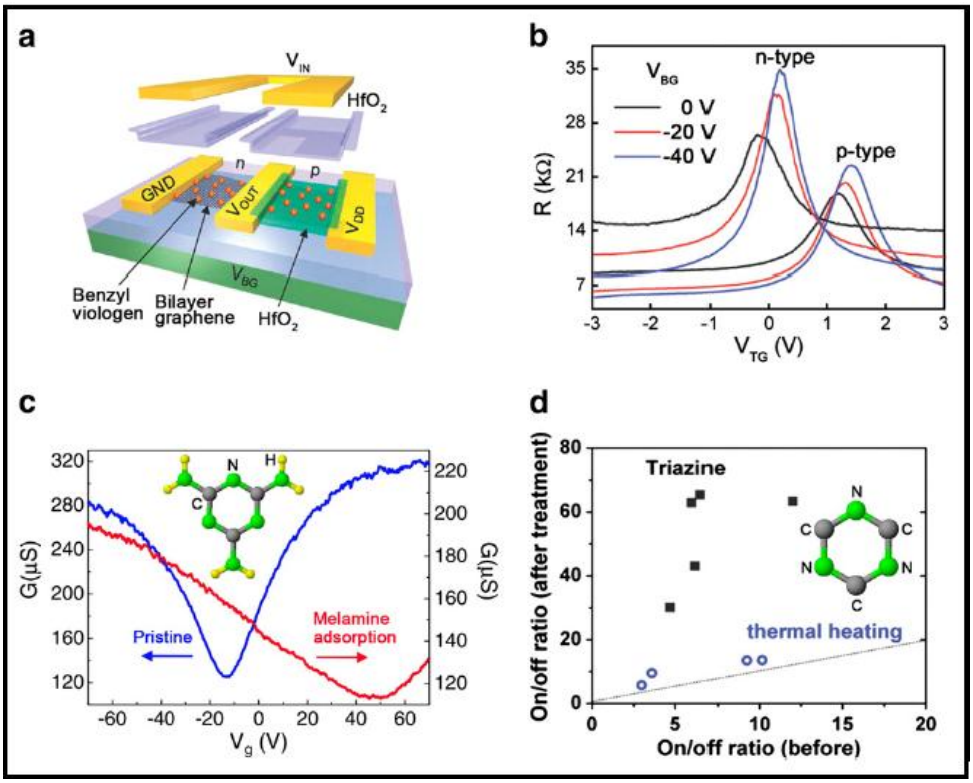

Fig. 2.1: Molecular doping of graphene sheets. (a) Benzyl viologen (BV)-doped bilayer graphene transistor and (b) switching behavior of n-type (BV-doped) and p-type (pristine) bilayer graphene FETs as a function of top gate voltage (VTG) at different bottom gate voltages [95]. (c) Conduction of graphene FET devices before (blue curve) and after (red curve) melamine molecular doping. The Dirac point moves from −12 to 50 V after doping [116]. (d) On/off current ratios for bilayer graphene FET devices before and after various treatments including triazine doping and 150 °C thermal annealing in vacuum [117]. The insets in (c) and (d) show the molecular structures of melamine and triazine, respectively.

2.2: CHARACTERIZATION

Graphene is single layer of graphite; all the carbon atoms in graphene are sp^2 hybridized and combined to form 2D honeycomb lattice crystal. If we look at electronic configuration of carbon then we find that initially each atom has two electrons in 2s orbital and two electron in $2p_x$ $2p_y$ $2p_z$. When hybridization occurs then one electron shifts from 2s orbital to $2p_z$ orbital. During bonding three hybridized sp^2 orbitals form sigma bonds with nearest carbon atoms which are responsible for the mechanical properties of lattice. Fourth $2p_z$ orbital is perpendicular to the plane of molecule hybridizes to form the π * (conduction) and π

(valence) bands. Pi bond is weaker than sigma bond and contributes for electrical properties of graphene [118]. There are many techniques and instruments which are used to characterize the properties of material. Some of them will be discussed here.

2.2.1: Optical Microscope

Many techniques have been used to characterize MFLG i.e. optical microscope, atomic force microscopy (AFM), transmission electron microscopy (TEM) and scanning electron microscopy (SEM). Frequently, two or more techniques are combined to imagine the few layer graphene (FLG).

Optical microscope is the instrument which is cheap and easily available in the laboratories, after the discovery of graphene this instrument was firstly used to image graphene layers. In this technique substrate is required, here graphene is mounted on the silicon dioxide substrate which produces good contrast images [119-121].

Mechanism:

In the dielectric surface layer, contrast mechanism is described using Fabry-Perot interference. Fabry–Perot interference is governed by intensity of Fluorescence which permits the contrast between substrate and graphene layers. In Michelson contrast (C) relation [122] visibility of sheets is

$$C = \frac{R_{material} - R_{dielectric}}{R_{material} + R_{dielectric}}$$

Where

$R_{material}$ = reflected intensity with the material

$R_{dielectric}$ = intensity deprived of the material

If value of C is zero then material is undetectable; however, if values of C varies from zero to one then material will be brighter as compared to the substrate and if value of C is zero or in minus then the sample will appear darker as compared to substrate.

Optical images of micromechanically exfoliated graphene with different layers are shown in the Fig. 2.2. AFM and color contrast is very helpful in determining the number of layers [123]. Therefore wavelength of incident light and thickness of substrate are very important for detection mechanism. In order to get the images of graphene without substrate, a lot of research is desired to be done.

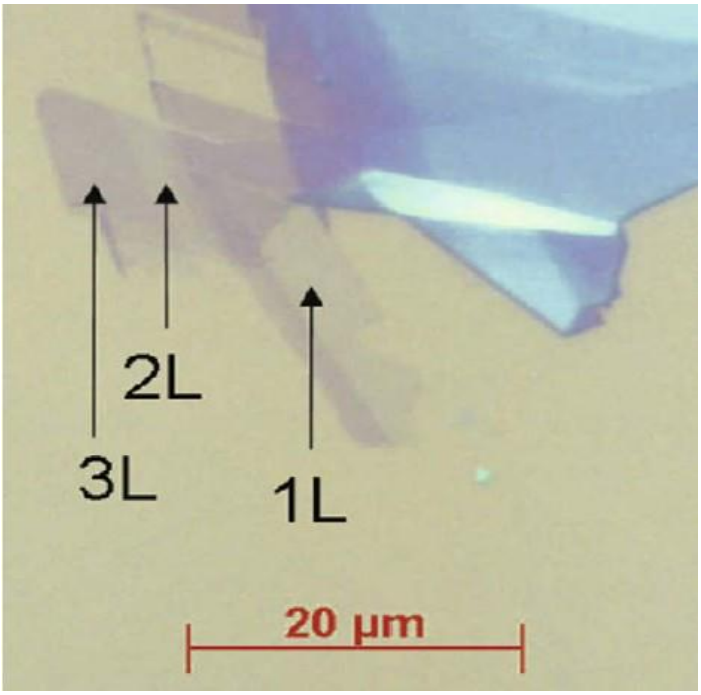

Fig. 2.2: Optical microscopy image of single-, double- and triple- layer graphene on Si with a 300 nm SiO_2 over-layer, labeled in the paper as 1L, 2L and 3L, respectively [123].

2.2.2: Atomic Force Microscopy (AFM)

The thickness of graphite flakes can be determined by using AFM where single layer is one atom thick, AFM technique can determine the thickness of material at Nano scale. Although images obtained by AFM give only topographic contrast which make it difficult to distinguish between graphene layers and graphene oxide, but differentiation between pristine graphene (defect free) and its functionalized pristine graphene is done by using its phase imaging feature. The difference of interacting forces which are created between AFM tip and functional group which are attached to it might be the reason of phase imagining feature. Paredes et al.[124] revealed the effect of gorgeous mode of AFM during the process of calculating sheet thickness, they also revealed height error which was produced due to deformation of repulsive mode. The thickness of unreduced GO was observed to be 1.0nm and 0.6nm for chemically reduced GO. Fig. 2.3 shows difference in the phase contrast and thickness, this difference was produced during the reduction process and due to different oxygen functional groups which leads to the difference in hydrophilicity.

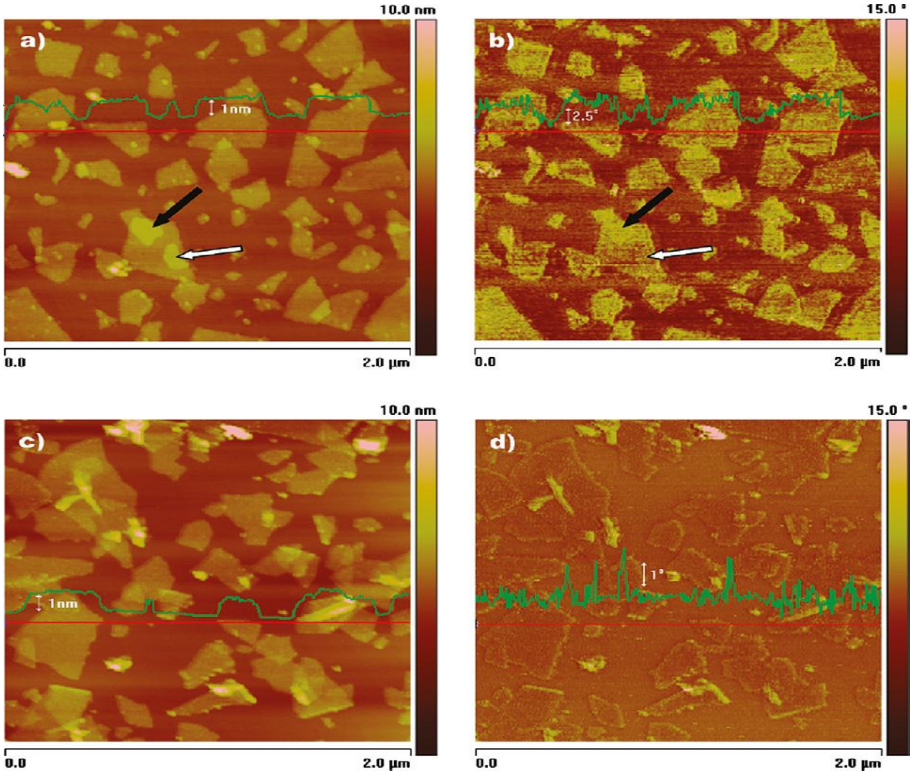

Fig. 2.3: Height (a, c) and corresponding phase (b, d) tapping-mode AFM images of unreduced (a, b) and chemically reduced (c, d) graphene oxide nanosheets deposited from aqueous dispersions onto freshly cleaved HOPG. The images were recorded in the attractive regime of tip sample interaction. Superimposed onto each image is a line profile taken along the marked red line [124].

For studying the electrical, mechanical and magnetic properties etc of graphene flakes AFM is used in different modes.

2.2.3: Transmission Electron Microscopy (TEM)

This technique is very helpful at atomic scale where low magnification images are required. TEM can be used to characterize the structure of suspended graphene, as shown in Fig. 2.4. Also due to single atom thickness of graphene enable suspended graphene film to investigate the defect sites during spherical aberration corrected TEM [125-128], and also adsorbed atoms which are very light such as carbon and hydrogen [129].

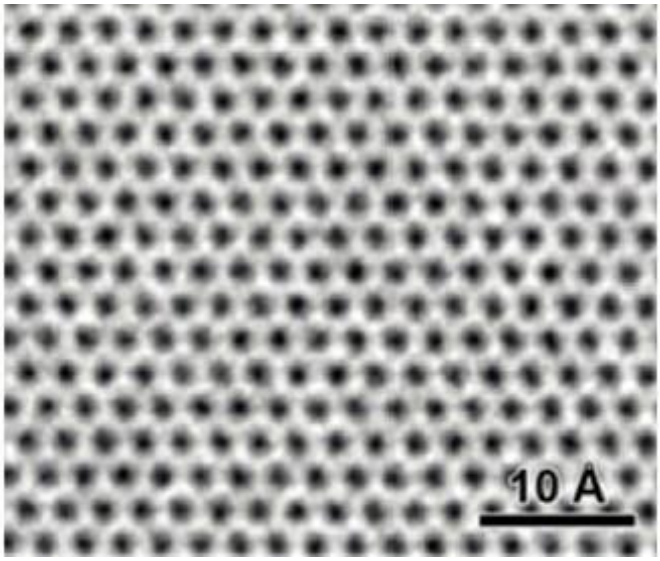

Fig. 2.4: Transmission electron microscopy (TEM) image of graphene[129] .

Normally TEM is operated at high voltage which might damage the monolayer while at low voltage resolution is not effective therefore its usage is limited. Recently some scientists used a new type of TEM, in this type of TEM 1Å resolution is provided at operating voltage of 80 kV [130, 131] where an aberration corrected in combination with mono chromator provides the above resolution. First-time direct high resolution graphene images were prepared by Mayer's group [129].

2.2.4: Raman Spectroscopy

Interactions between Electron and phonon which infer a high sensitivity for electronic and crystallographic structures can be viewed directly using a fast and non-damaging instrument, known as Raman microscope. Carbon allotropes give Raman microscopy typically by D peak (1350 cm^{-1}), G peak (1580 cm^{-1}) and 2D peak at 2700 cm^{-1} which are caused by change of electronic band structure. In this way we can determine the number of layers, concentration of doping, strain effects, effect of defect presence and temperature.

Ferrari et al. [132] investigated the Raman images of mono, bi, tri and few layer graphene. During his experiment they used the scotch tape method to produce graphene. He got the clear and good quality signals for mono, bi, tri and few layer graphene (less than five layers), therefore in this way Raman spectroscopy became very attractive and useful technique for graphene and GNRs characterization.

Raman microscope is used to investigate and characterize all kinds of carbon structures. The most important feature of Raman microscopy is band due to sp^2

hybridized carbon constituents are the G-band which appear at ca.1580 cm^{-1} and G'-band (2D-band) at ca. 2700 cm^{-1} when 2.41 eV laser excitation energy is used. D-band, at ca.1350 cm^{-1} is due to disorder and boundaries within same structure. The G-band is related with the doubly degenerate (iTO and LO) phonon mode (E_{2g} symmetry) at the center of Brillouin zone. On the other hand, the 2D-band the D-bands created from second-order processes, including two iTO phonons near the K point for the 2D-band or one iTO phonon and one defect for the D-band [133].

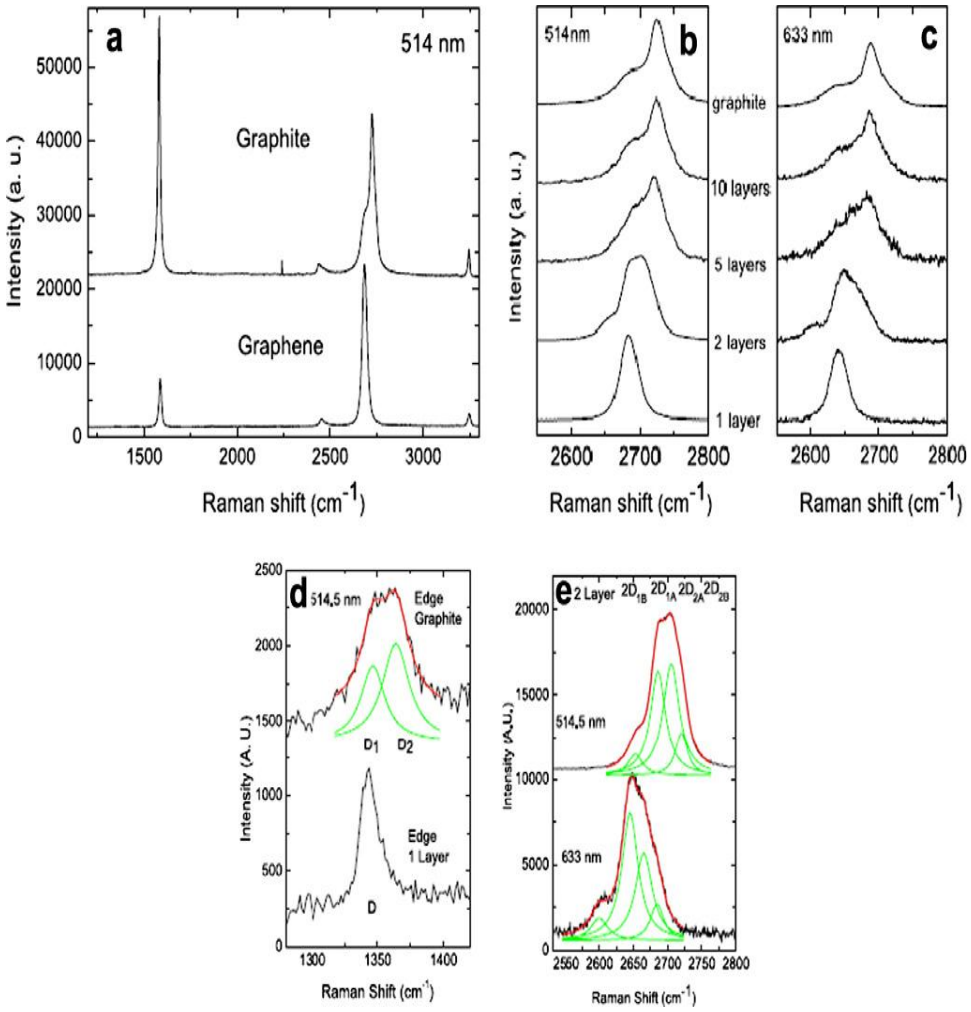

Fig. 2.5: (a) Comparison of Raman spectra at 514 nm for the graphite and single layer graphene, (b, c) Evolution in 2D band as a function of layers at 514 and 633 nm excitations, (d, e) Comparison of the D band at 514 nm at the edge of bulk graphite and single layer graphene. The fit of the D1 and D2 components of the D band of bulk graphite is shown in (e). Four components of the 2D band in 2 layer graphene at 514 and 633 nm [132].

Ferrari investigated that 2D-band have different peak shapes for mono, bi, and few layer graphene, such kind of graphene is prepared from the highly oriented pyrolytic graphite by using scotch tape method, so it contains AB Bernal stacking [132]. In case of single layer graphene 2D-band is at 2700 cm^{-1} having a FWHM of 24 cm^{-1}. It was observed that intensity of 2D-band is greater that the intensity of G-band. Bi layer graphene have 2D-band having four excitations. Five layer graphene have very similar spectra to that of bulk graphite and very hardly distinguished. The Raman spectra of single to few layer graphene and of graphite are compared in Fig. 2.5.

Chapter 3 Experimental Work

3.1 Aim and Scheme of Work

The aim of this work includes (1) - The characterization of doped and un-doped mono and few layer graphene sheets and study of their properties (2)- To study the dependence of doping effect on thickness of graphene sheets (3)- To realize the graphene as surface-enhanced Raman scattering (SERS) substrate for the identification of trace quantity Sudan IV dye for the first time. And (4) to induce band gap in graphene by doping with Methyl Orange (MO).

For the characterization of graphene sheets several techniques are used. The main techniques used include optical microscopy, Atomic Force Microscopy (AFM), Scanning Tunneling Microscopy (STM), Scanning Electron Microscopy (SEM), Raman Spectroscopy and U/Vis Spectroscopy. The graphene layers exhibit color contrast phenomenon on Oxidized Silicon substrate (300nm SiO_2 give good contrast). Optical Microscope was used for identification of mono and few layer graphene by color contrast. The numbers of graphene layer are easily identified by their unique colors. The second and better differentiation among graphene layers can easily be done by Atomic Force Microscope (AFM) and confirmation of graphene layers can be done by Raman Spectroscopy. Scanning Electron Microscope (SEM), AFM and Scanning Tunneling Microscope (STM) were used for EDX analysis and surface topography, respectively.

Raman spectroscopy is outstanding device for studying graphene, as it can be used for identifying the number of layers, distinguishing the type of doping, probing strain, providing the defect information, probing the electronic structure of graphene, identifying the edge orientations and stacking orders. It was used for distinguishing type of doping, studying the thickness dependence of doping effect of graphene sheets and Surface-enhanced Raman scattering (SERS) study of graphene. For the first time, SERS of Sudan IV molecules on the few-layer graphene (FLG) was used for the identification and analysis of trace quantity of Sudan IV molecules. UV/Vis Spectroscopy was used for band gap study of pristine and doped graphene.

3.2 Material and Method

Highly Oriented Pyrolytic Graphite (HOPG) was used as graphene source. Single side polished thermally oxidized Silicon wafer (300 nm SiO_2 layer) was used as

substrate on which graphene sheets produce color contrast [134]. Adhesive tape was used to transfer mono and few layer graphene sheets on Si/SiO_2 substrate. Si wafer was cut into pieces with diamond cutter. Cleaning of substrate was done in ultra-sonication bath with ultra-pure water, ethanol, H_2SO_4, H_2O_2 and HF solution. Nitrogen gas was used for drying of samples. The dimethyl formamide (DMF) was used for making molar solution of Methyl Orange (MO) in measuring flask. Digital weight balance was used for weighing Methyl Orange. Spin coater was used for the uniform adsorption of MO on the graphene sheets.

3.3: Experiments and studies performed

Distinguishing of mono and few layer graphene sheets

(1) To distinguish mono and few layers graphene by color contrast

(2) Determination of mono and few layers graphene by AFM and Raman Microscopy

Study of Effect of doping parameters

(3) Topographic and EDX study of few layers graphene

(4) (a)-Doping of mono and few layers graphene, study of effects of doping and

(b)- Surface-enhanced Raman scattering (SERS) of Sudan Red IV on graphene substrate

(5) To induce band gap in few layer graphene by doping.

3.3.1: To distinguish mono and few layers graphene by color contrast

STEP#1: Cutting and washing of substrate

Different substrates can be used for graphene but the most useful substrate is Si/SiO_2, as different graphene layers produces different color contrast on this substrate and can be easily identified by their unique color. For this purpose we used single side polished thermally oxidized Silicon wafer as substrate. The silicon wafers were brittle and were cut into $4cm^2$ pieces by diamond cutter. Then these pieces were cleaned by series of steps as followed; first substrate pieces were washed with ultra-pure water and then were sonicated in ethanol for 15 minutes. Then again were washed with ultra-pure water for one minute and then were immersed in 1:1 H_2SO_4 and H_2O_2 solution for 10 minutes. For hydrogen termination these pieces were washed in HF solution for 1 minute and then dried with nitrogen gas.

STEP#2: Preparing of Samples

Graphene was obtained from Highly Oriented Pyrolytic Graphite (HOPG) and swatch tap was used to mount few layers' flakes on silicon substrate. Firstly adhesive tape was stuck on HOPG and when removed had thick sheet of graphite. Then peel off process was done dozen of times to get lesser and lesser number of graphite flakes. This process continued till single layer graphene sheet was obtained. Then tape was pasted on the silicon substrate containing 300 nm thick oxide layer (SiO_2) and rubbed over by fingertip. When tap was removed slowly, it leaves mono and few layer graphene sheets. These samples were analyzed under optical microscope.

3.3.2: Determination of mono and few layers graphene by AFM and Raman Spectroscopy

The same samples which were used for Optical Microscopic study were subjected to Atomic Force Microscopy (AFM) and Raman Spectroscopic analysis. AFM has been used for measuring the thickness of observed graphene sheets. The scanning step height gives the idea of number of layers of graphene sheets and is considered as a good tool to determine the number of graphene layers. The most reliable tool for the determination of number of graphene layer is Raman Spectroscopy.

3.3.3: Topographic and EDX study of mono and few layers graphene

The same method as discussed in Experiment 1 for preparation of samples for SEM and AFM analysis (except for STM analysis) was used. After cleaning of the substrate graphene sheets were used after mounting by swatch tap. These samples were carried out for AFM and SEM analysis. For analysis of surface topography and lattice defects using Scanning Tunneling Microscopy (STM), steel coin was used as substrate. Same steps were repeated for cleaning and preparing samples as in Experiment 1. Doping of graphene was also done and EDX was carried out.

3.3.4: a. Doping of mono and few layers graphene and study of effects of doping

b. Surface-enhanced Raman scattering (SERS) of Sudan Red IV on Graphene Substrate

The doping of mono and few layer graphene sheets on Si/SiO_2 substrate was done with methyl orange (MO) and Sudan Red IV. Dimethyl formamide (DMF) was used as solvent for preparation MO solution of three different concentrations 2×10^{-3} M, 2×10^{-5} M and 2×10^{-7} M. Whereas, only 2×10^{-5} M solution of Sudan Red IV was prepared in DMF. Both MO and Sudan Red were adsorbed on graphene sheets by spin coating with 1000rpm speed, by taking 25 $\mu L/cm^2$ volume of as prepared

solution. After drying, these samples were rinsed with distilled water. Sudan Red IV doped samples were subjected to Surface Enhanced Raman Spectroscopy (SERS) study on graphene substrate and trace quantity detection Sudan IV molecules for the first time.

3.3.5: To induce band gap in few layer graphene by doping.

Pure graphene has zero band gap and for electronic applications it is desired to increase the band gap in semi conducting range. The graphene layers are very smooth. Doping was used to induce band gap and creating defects in graphene layers. The samples were prepared with the same method as in Experiment 4. The prepared samples were subjected to UV/Vis Spectroscopy band gap measurements. Naked Silicon substrate was used as reference to exclude its effect in the measurements. Then un-doped graphene and doped graphene samples were analysed for band gap determination.

3.4: Characterization Techniques Used

There are several techniques available for the characterization of graphene and functionalized / doped graphene among which some are qualitative and other are quantitative analysis. The qualitative analysis gives general information (overview) of the property of interest without providing numerical values whereas quantitative analysis gives numerical measure of properties of the material. Spectroscopy analysis gives information like how compounds absorb different type of energies; on the other hand chromatography separates molecules on the basis of characteristics such as charge or size. The surface analysis of materials under microscope is a qualitative technique. There are many surfaces that are chemically active so to prevent from contamination we need some definite preparation procedures or equipment. Irrespective of such problems, for surface analysis we have developed large range of characterization methods.

We used following characterization tools.

(1) Optical Microscopy
(2) Atomic Force Microscopy (AFM)
(3) Scanning Electron Microscopy (SEM)
(4) Scanning Tunneling Microscopy (STM)
(5) Raman Spectroscopy
(6) UV/Vis Spectroscopy

3.4.1: Optical Microscopy

High resolution optical microscope, OPTIKA was used in Optical Microscopy Laboratory at SCME for optical imaging of graphene sheets. Camera was used to capture the optical images taken by microscope and the results were saved in computer coupled with microscope and camera. The magnification power of the microscope used was 1000X. The mono and multi-layer graphene sheets were distinguished by color contrast as graphene sheets produce excellent color contrast on Si/SiO_2 substrate. Mono and few layer graphene was distinguished by their unique color, which vary from purple to yellow,

3.4.2: Atomic Force Microscopy (AFM)

The AFM analysis of pristine graphene and doped graphene was performed using JEOL Japan, JSPM 5200 Scanning Probe Microscope at SCME. The AFM have the resolution in nanometers, less than 1 nm. The AFM gives topographic analysis but we can also calculate the number of graphene layers by step height.

3.4.3: Scanning Electron Microscopy (SEM)

The SEM analysis of doped and undoped graphene sheets was performed using JEOL Japan, JSM 6490A analytical electron microscope. The resolution of SEM machine was up to few nanometers and its magnification range was about 10-3000, 000. The surface topography of graphene flakes and the Si/SiO_2 substrate was performed by SEM and in addition to topography of surface under observation; it can also provide composition of the surface by energy dispersive spectroscopy (EDX). As the oxidized silicon surface does not conduct charge, also graphene sheet are not covering the surface of substrate. So the charge accumulation occurs and image turn blurred. To overcome this problem whole sample was coated with 200 A^o thick gold layers by JFC 1500 ion sputtering device which made sample surface conducting. The topographic study of graphene sheets of varying thickness was performed and EDS of selected few layer fake surface was done. Topographic and EDX analysis of doped graphene sheets were done after spin coating the doping spices. SEM analysis was performed to get information about shape & surface morphology, particle size, packing and composition.

3.4.4: Scanning Tunneling Microscopy (STM)

Surface morphology and atomic structure analysis was carried out with Scanning Tunneling Microscopy (STM). The atomic structure of graphene and surface morphology was analyzed by STM. However the resolution achieved was not enough for atomic structure.

3.4.5: Raman Spectroscopy

The confirmation of number of graphene layers was done using Raman Spectroscopy. Furthermore, Raman Spectroscopy was used to analyze doping effect and Surface Enhanced Raman Scattering (SERS) spectra were used for the detection of Sudan Red IV on few layer graphene sheets.

Raman spectroscopy (Renishaw in Via plus, He-Ne laser, 632.8 nm, 100% laser power, 50× magnification) was used for Raman and SERS spectra.

3.4.6: UV/Vis Spectroscopy

Band gap measurement was done by UV/Vis spectroscopy at SMME Lab. Doping of mono and few layer graphene with methyl orange was done to open the band gap of graphene. Firstly, absorbance spectrum of reference Si/SiO_2 substrate was subtracted and then absorbance spectra for undoped and doped graphene sample were collected over entire visible spectrum wavelength range.

Chapter 4 Results and Discussion

4.1: To distinguish mono and few layers graphene by color contrast

Despite the micromechanical cleavage is simple technique to get graphene; major issue is the identification of mono and few layer graphene. This technique produces very few sheets of single layer graphene among the large number of thick flakes. However, single and few layer graphene produces color contrast due to interference phenomenon on oxidized (typical 300nm thick oxide layer) surface on the silicon substrate.

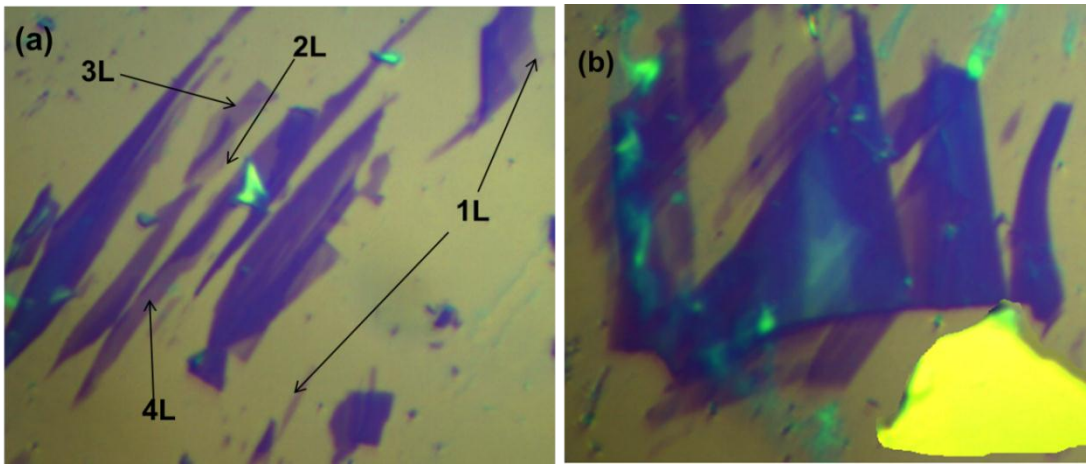

Figure 4.1: Optical images of mono and few layer graphene sheets on oxidized silicon substrate (300nm thick Oxide layer)

The graphene flakes of different color are visible in Figure 4.1 (a & b); there exists a thin layer of graphene sheet at the top surface of thick graphene flake. Light purple color is due to mono layer graphene sheets; however with increase in graphene layers increase the color goes darker and darker. As the purple color turn dark the number of layers reached up to nine. When number of layers increases over 10, color of graphene sheets changes from light to dark blue, similarly yellow color results for thick graphene. The optical color contrast results due to interference between graphene layers and oxide layer on silicon substrate and very fine contrast was produced on typically 300nm thick oxide layer on silicon substrate (Si/SiO_2). In the Fig 4.2 different thickness graphene flakes are present but they didn't produce fine color contrast even very thin graphene sheets are present. However the thin flakes appear yellow, because the polished silicon substrate was oxidized in open air and produce faint color contrast.

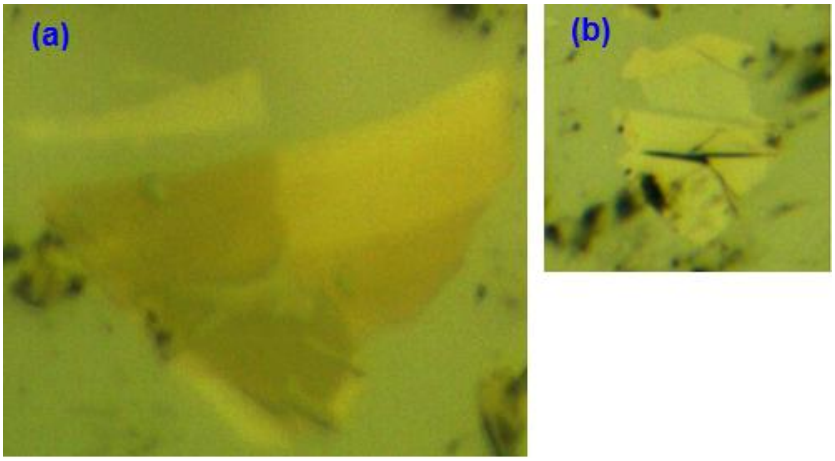

Figure 4.2: Optical images of graphene flakes on un-oxidized polished silicon substrate

4.2: Determination of mono and few layers graphene by AFM and Raman Spectroscopy

4.2.1: Atomic Force Microscopic Measurements

The atomic force microscopy has been used for measuring thickness of few layer graphene hence distinguishing few layer graphene. In figure 4.3, 2-dimensional and 3-dimensional AFM images of graphene flakes are shown. Where as in figure 4.4 thickness of few layer graphene has been measured using marker. The measured thickness of thin graphene sheet was 3.22nm which is about 10 layer thick graphene sheets.

In the Fig 4.5 and Fig 4.6 the 2-dimensional, 3-dimensional image and marked image of few graphene flake has been shown. The measured thickness of marked part of the graphene flake was 0.364 nm which is the thickness of mono layer graphene. However this mono layer flake is very small. The thickness of graphene sheets can't be identified exactly by AFM, the reason is that the graphene sheets show different adhesive forces with different substrates. Therefore precise measurement of graphene thickness is done by Raman Spectroscopy.

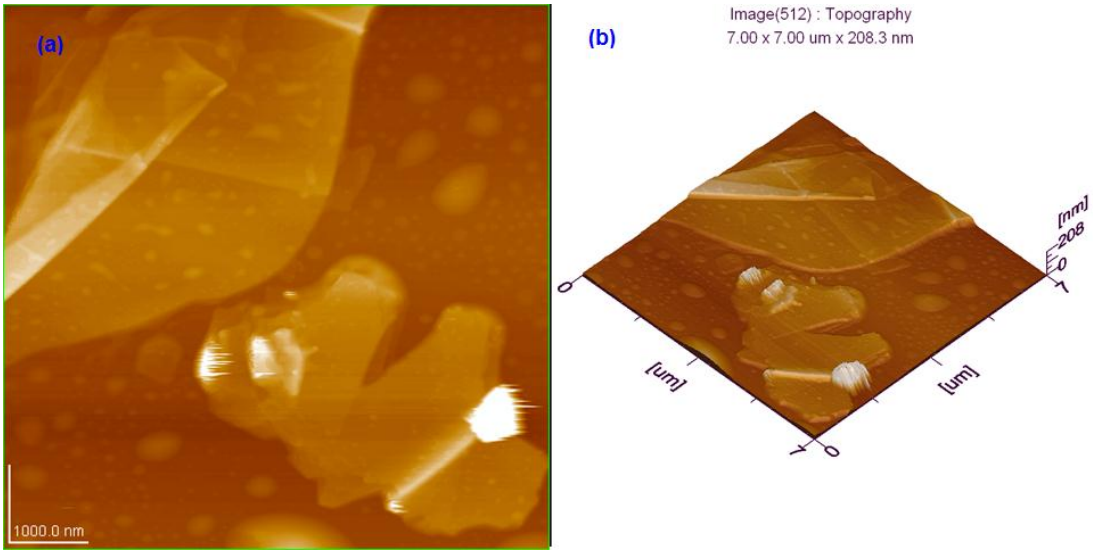

Figure 4.3: AFM images of 2-dimensional (a) and 3-dimensional (b) view of few layer graphene sheets.

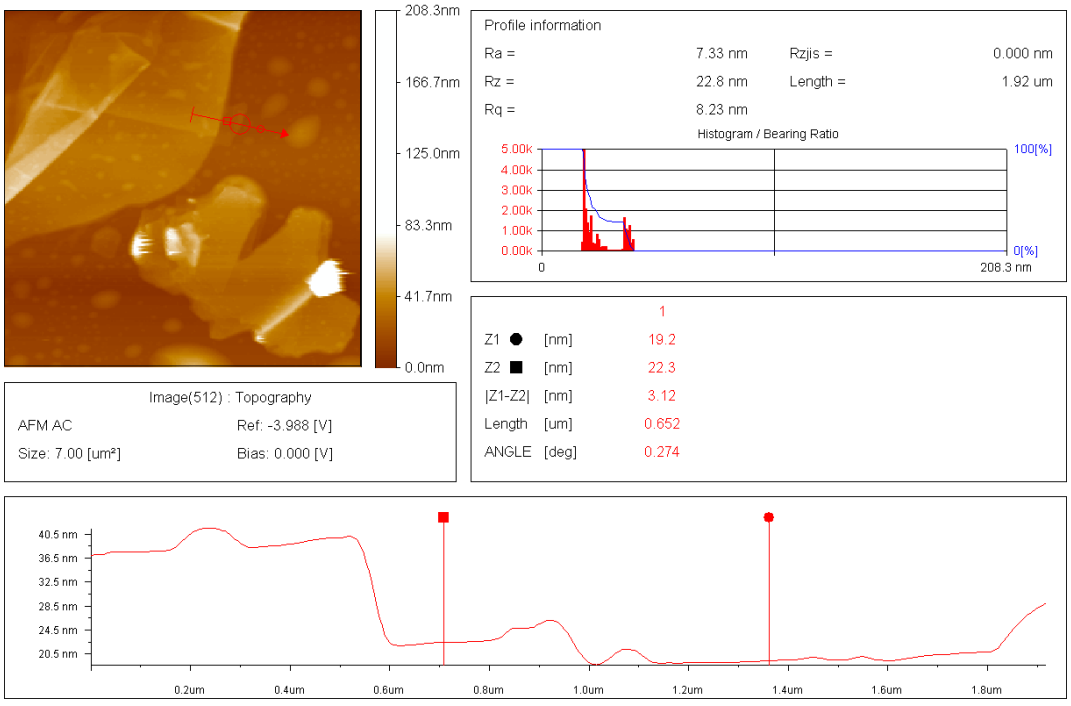

Figure 4.4: Measurement of thickness of graphene sheets by step height in AFM scan

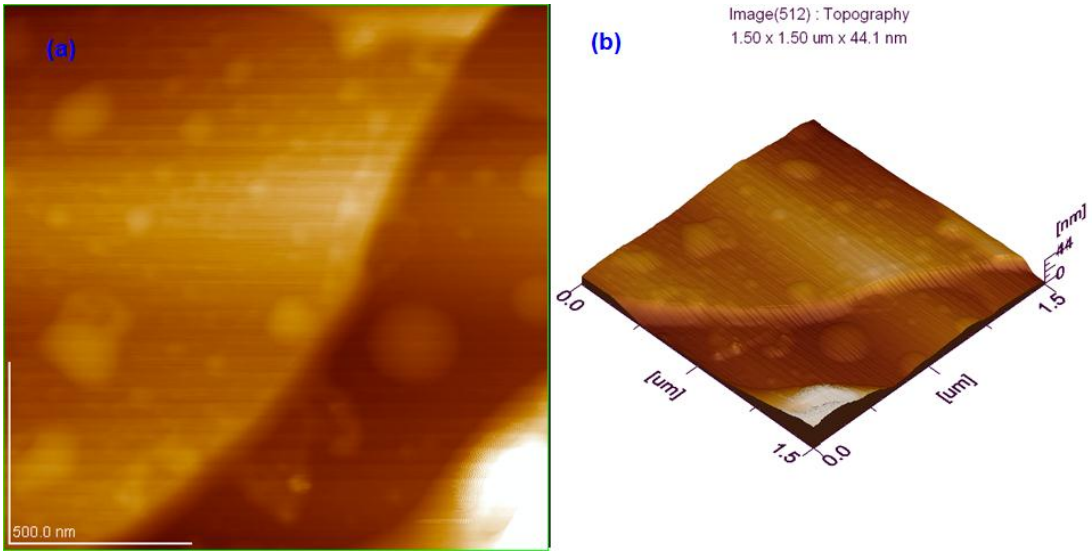

Figure 4.5: AFM images of 2-dimensional (a) and 3-dimensional (b) view of few layer graphene sheets.

Although for the identification of graphene layers atomic force microscopy (AFM) is considered as the easiest way. But this is very slow process and it can damage the graphene crystal lattice. Another problem with this method is the existence of instrument offset error of 0.5nm and this is greater compared to the thickness of single layer graphene sheet. To tackle with this problem we need to fit the data for determination of real thickness [135].

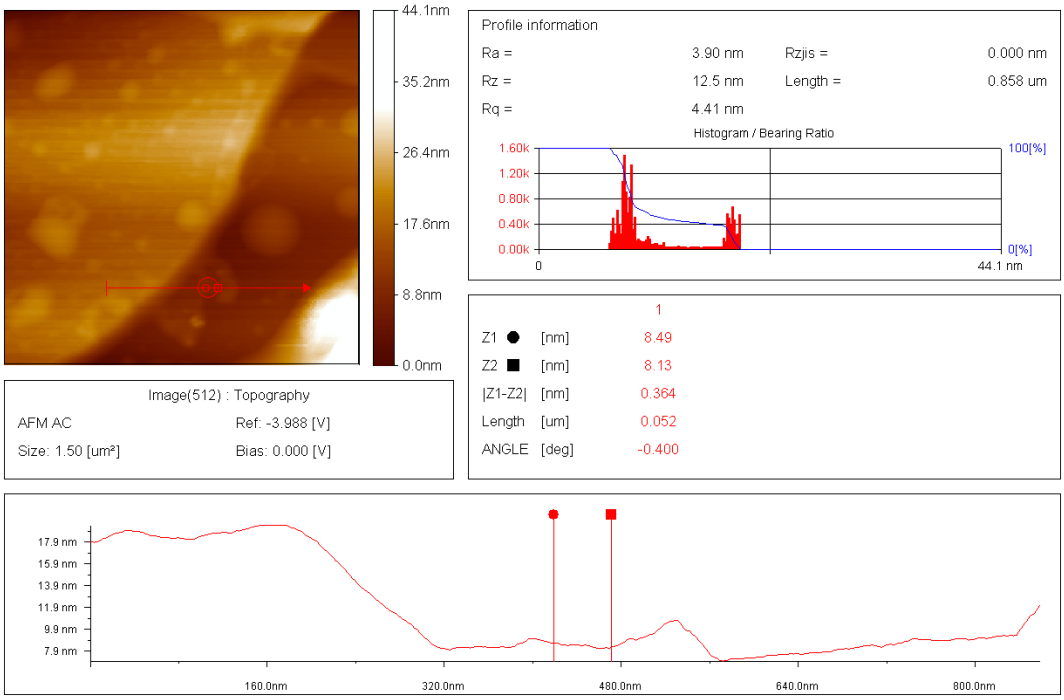

Fig 4.6: Measurement of thickness of graphene sheets by step height in AFM scan

The AFM used had a limitation of absence of CCD camera which could be used to locate the mono and few layer thick graphene flakes and taking measurement of right area for confirmation of number of graphene layers in the observed flake. So we had to use hit and trial method to get the least thick flake.

4.2.2: Raman Spectroscopic Measurements

Raman spectroscopy has been used for distinguishing the mono and few layer graphene. The G band intensity and 2D band width has been the tool for determining number of graphene layers. Pure graphene sheets of all thickness produce G band peak at 1580 cm^{-1} and is finger print of graphene and graphite. However the G band intensity varies with thickness of graphene. 2D spectrum of few layer graphene comes about 2670 cm^{-1} and its width and position varies with thickness of graphene sheets. However the doping can shift the position of both G and 2D band which can also be used to identify the number of graphene layers.

The Raman spectra of Methyl Orange doped mono and few layer graphene mounted on silicon substrate by scotch tap method are discussed in Experiment 4 (a).

4.3- Surface Topography and EDX study of mono and few layers graphene

4.3.1- AFM analysis

The AFM topographic analysis to analyze the surface roughness of graphene sheets has been performed. The Fig 4.7 2-dimensional and 3-dimensional images are shown. A thick graphene flake was observed in this image. The average surface roughness across the marked line was found to be 4.95nm in Fig 4.8.

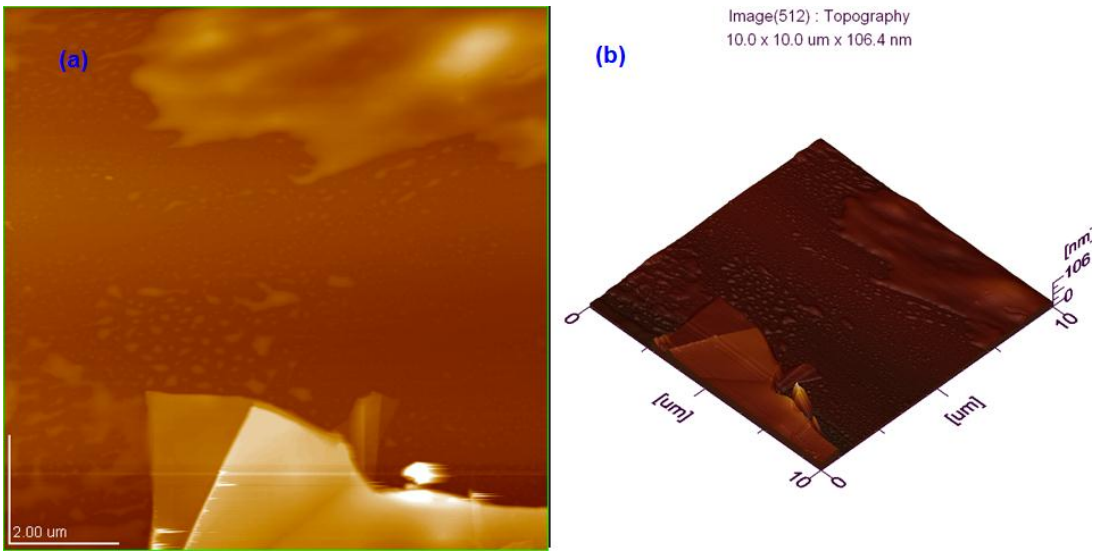

Fig 4.7: AFM images for surface morphology of few layer graphene sheets (a) 2-dimensional (b) 3-dimensional view.

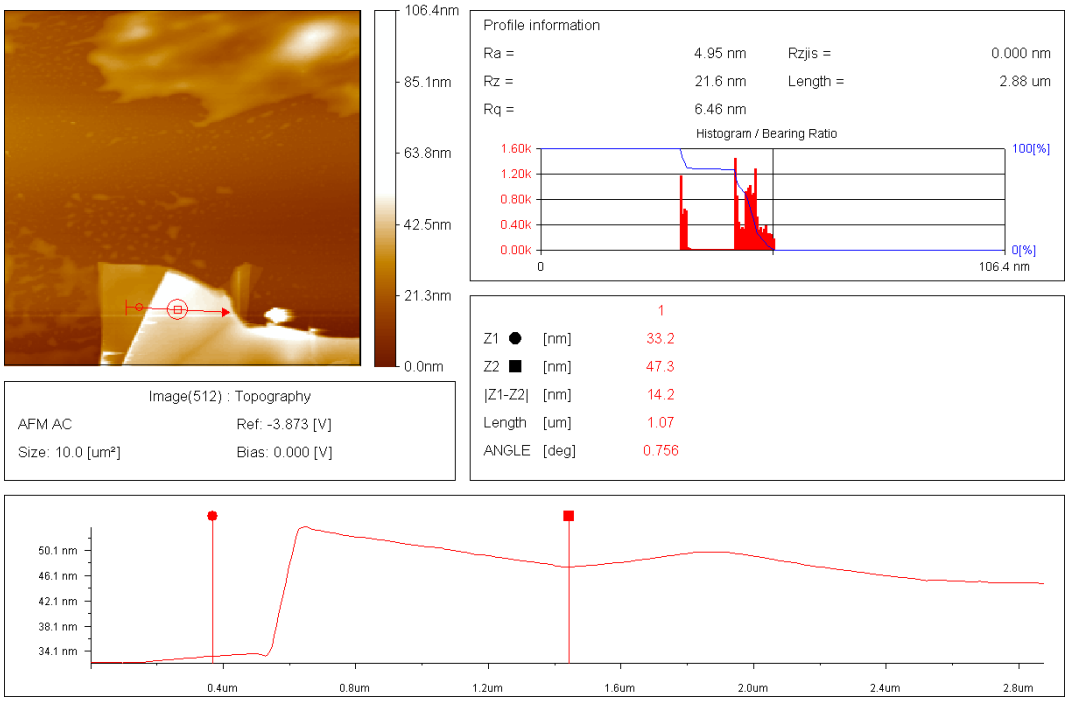

Fig 4.8: AFM images for surface roughness top surface of few layer thick graphene sheets

The Fig 4.9 shows 2-D & 3-D scanned images for surface topography of graphene flake and Fig 4.10 shows surface roughness measurement of observed flake. The average roughness across marked line reported was about 0.25 nm.

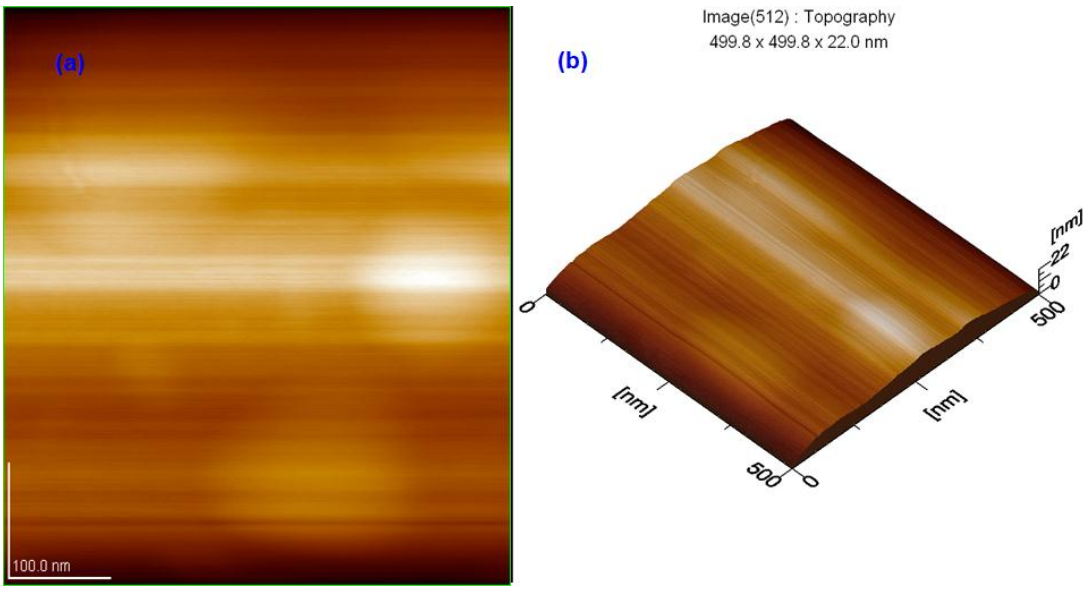

Fig 4.9: AFM images for surface morphology of few layer graphene sheets (a) 2-dimensional (b) 3-dimensional view.

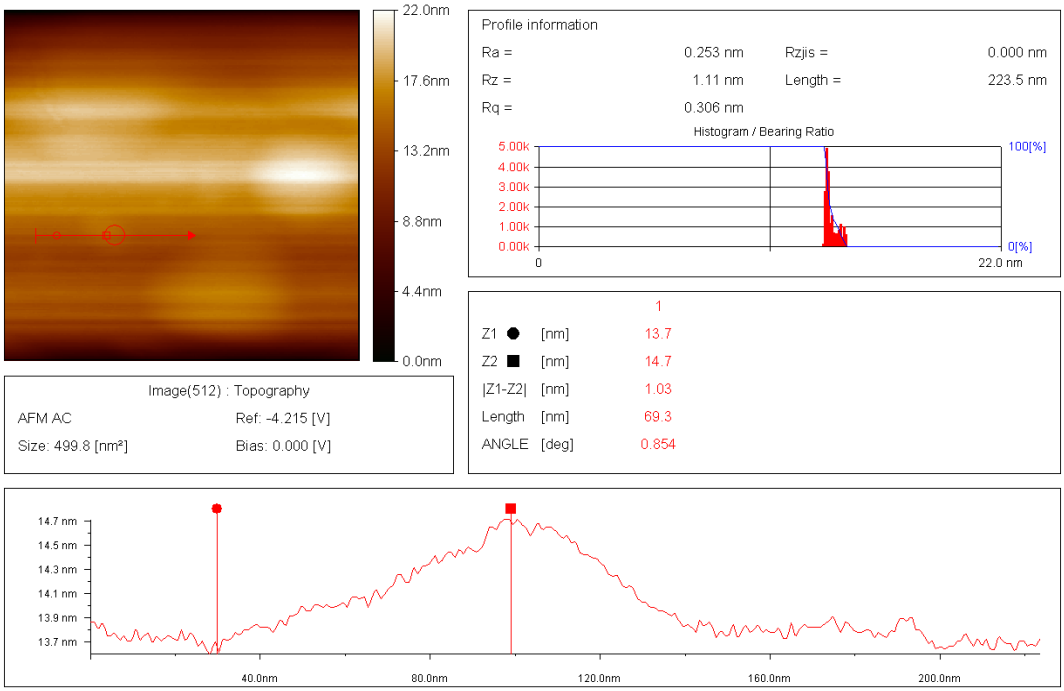

Fig 4.10: Surface roughness top surface of few layer thick graphene sheets by step height in AFM scan

4.3.2- STM Analysis for topography and lattice defect of graphene

The Scanning Tunneling Microscopy was used to study the topography and lattice defect study of graphene sheets. We tried to achieve atomic resolution by varying the scan time, z-range, scan area and sharpening STM tip. However the highest achieved resolution has been discussed as below.

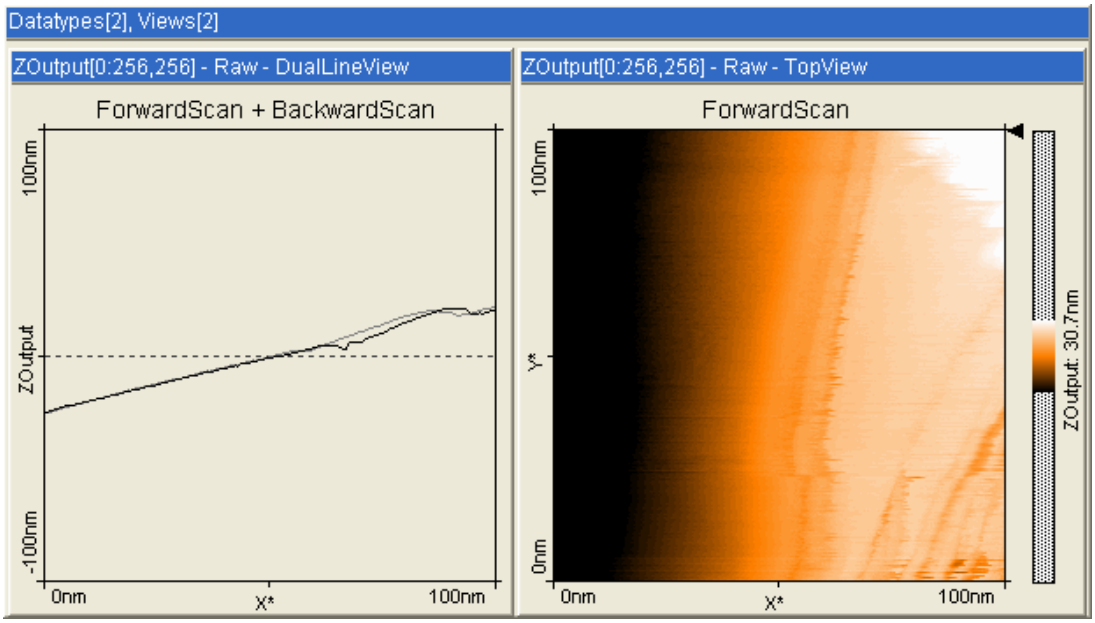

Fig 4.11: STM image for surface morphology of graphene sheet

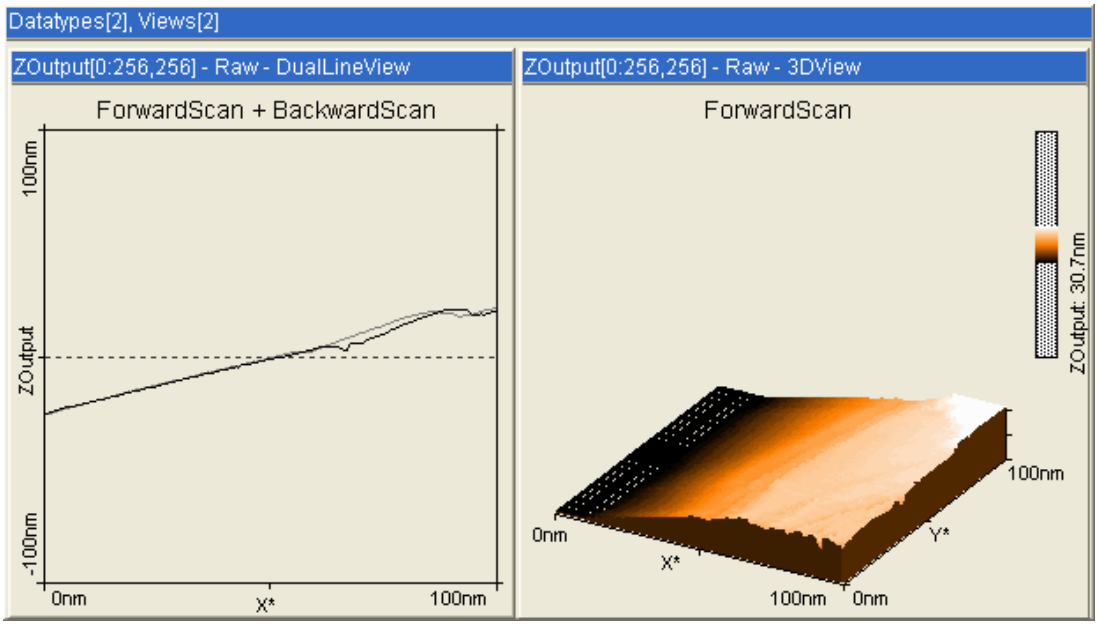

Figure 4.12: 3-diminsional STM image for surface morphology of graphene sheet

In Fig 4.11 and Fig 4.12 topography study was performed. The scanning time was 1.499 sec/line, scanning area was 100 nm and z-range was fixed at 200 nm. I and P gain was set at 12.

In Fig 4.13, Fig 4.14 and Fig 4.15 the scan range was set at 4.01 nm and z-range was 3.12 nm. The scan time was set at 1.0 sec/line with I and P gain 12. The relatively high resolution was achieved. The graphene surface lattice was observed to be defect free. The scan was slightly disturbed due to disturbances in the surrounding caused

by personals movements in laboratory as well as noise and floor vibrations. The scan images revealed the very smooth lattice graphene sheets having small defects.

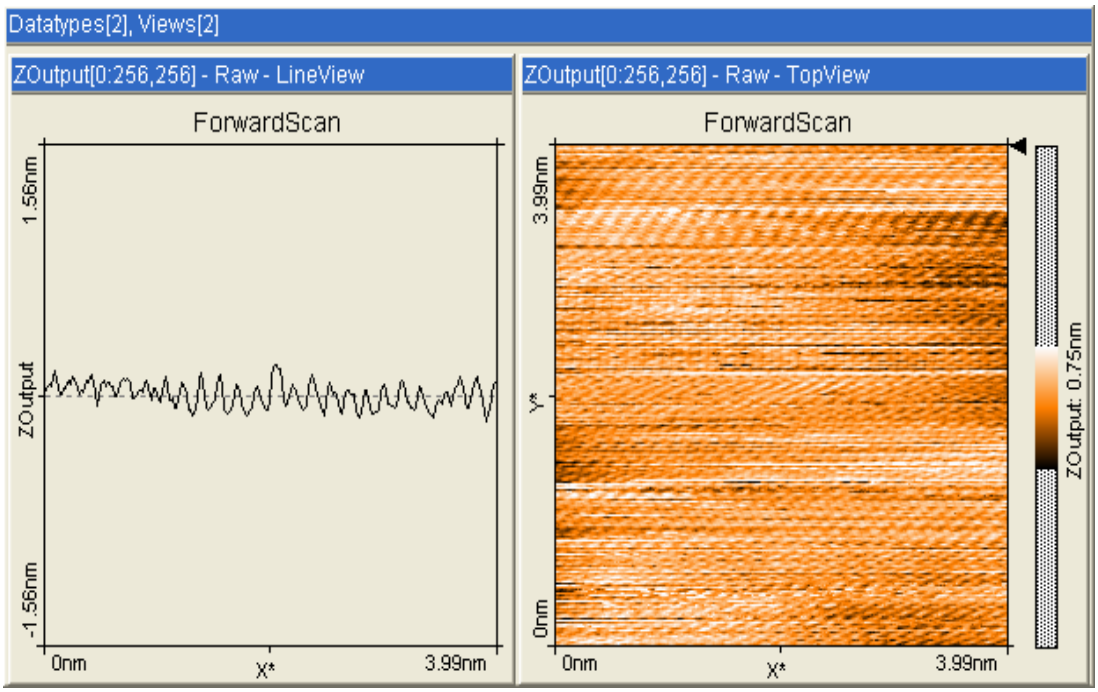

Fig 4.13: Highly resolved STM image for surface morphology of graphene sheet (bright contrast)

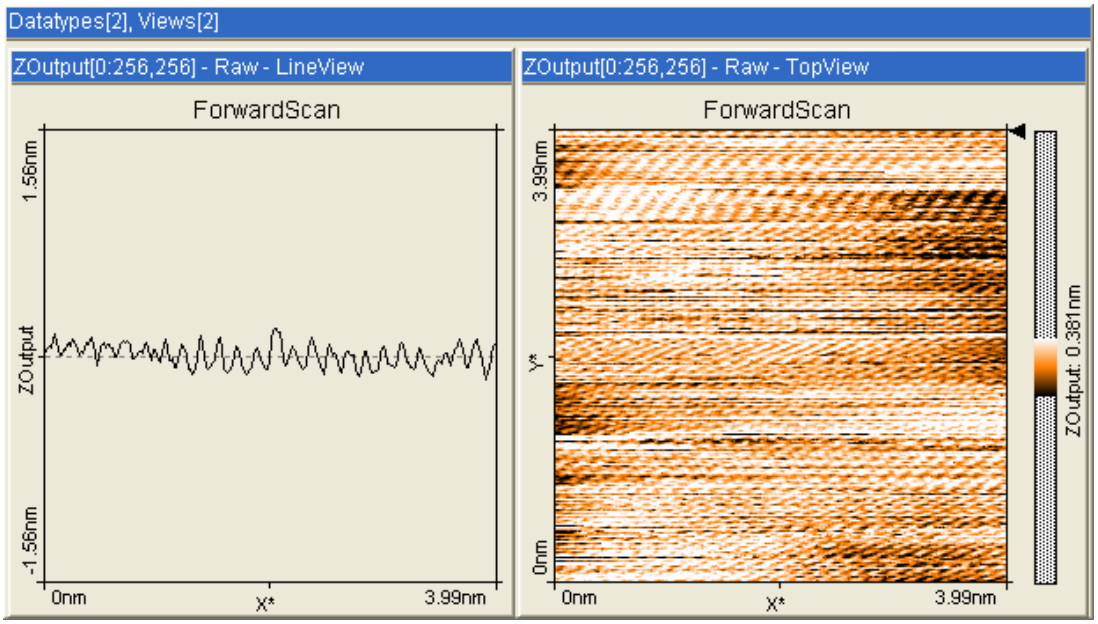

Figure 4.14: Highly resolved STM image for surface morphology of graphene sheet (dark contrast)

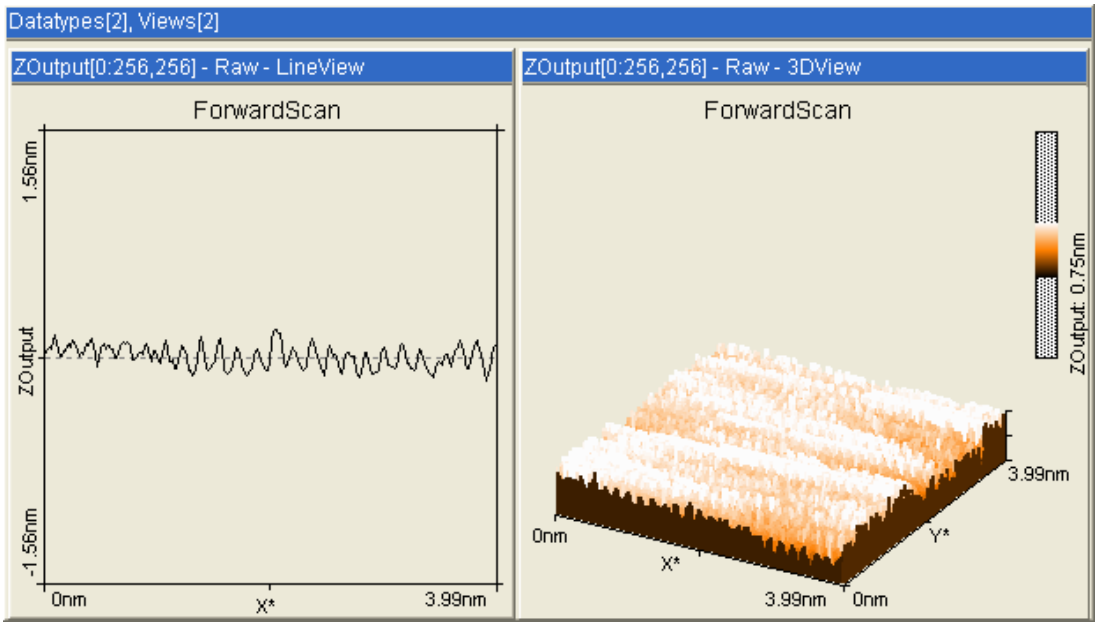

Figure 4.15: Highly resolved 3-diminsional image of surface morphology of graphene sheet (bright contrast)

In Fig 4.16 and Fig 4.17 scanning was performed with same parameter except scan time of 0.599 sec/line was carried out. The reason for short scanning time was, to avoid disturbances caused in surroundings. However in this scan resolution achieve was not fine.

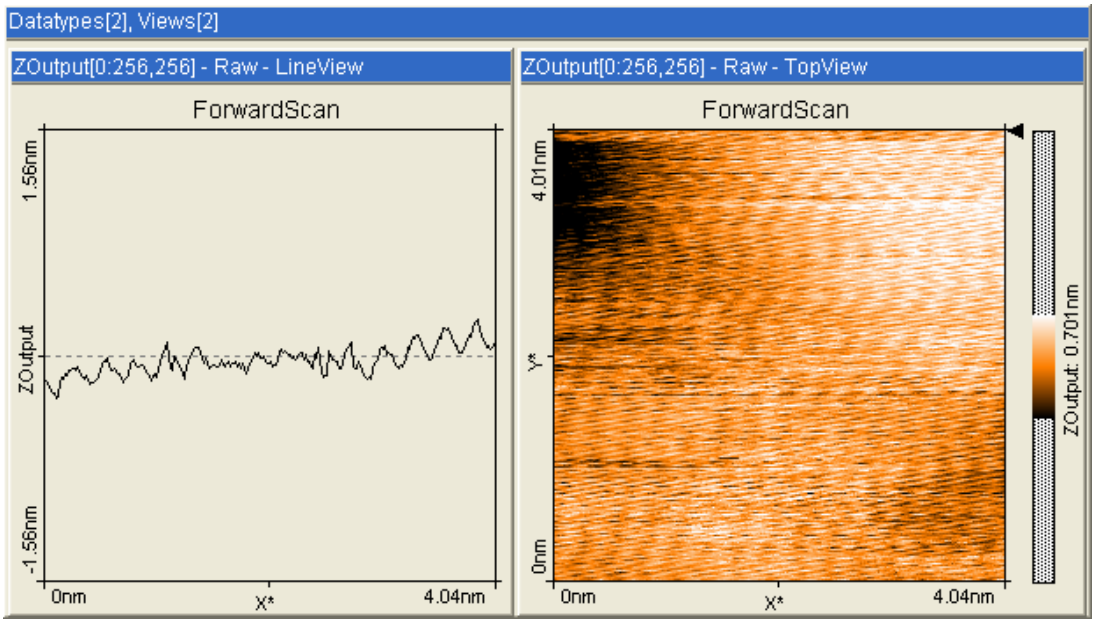

Figure 4.16: Highly resolved image of surface morphology of graphene sheet

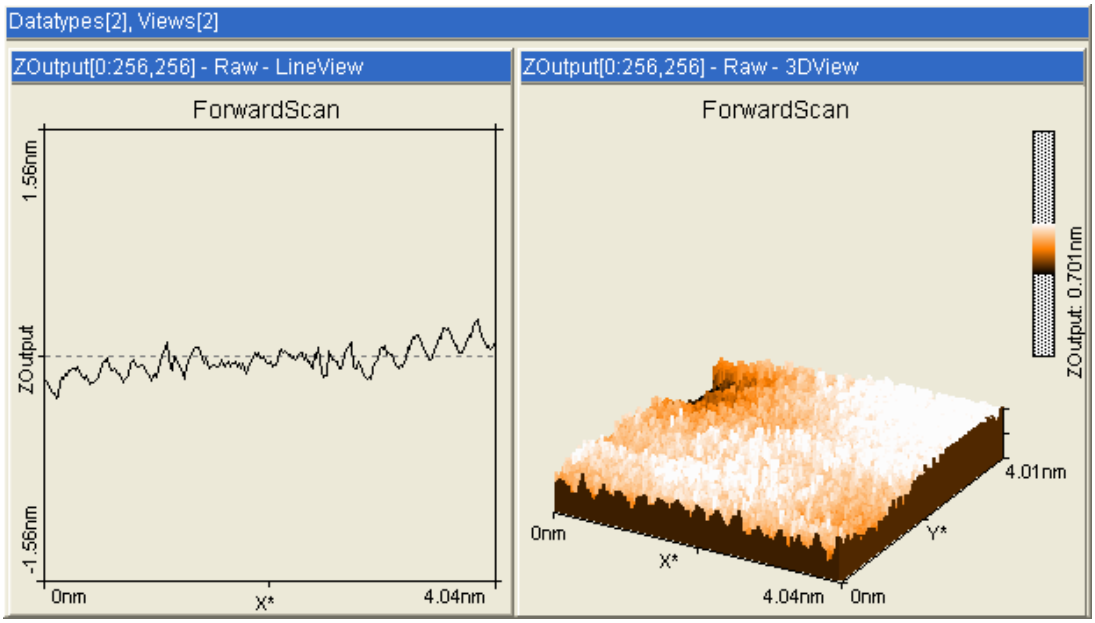

Figure 4.17: Highly resolved 3-diminsional image of surface morphology of graphene sheet

4.3.3- SEM surface topographic and EDX study

The surface morphology of pristine and doped graphene sheets with different concentrations was studied by scanning electron microscopy (SEM) at 1000x. Very smooth and transparent graphene flakes were observed in the SEM images.

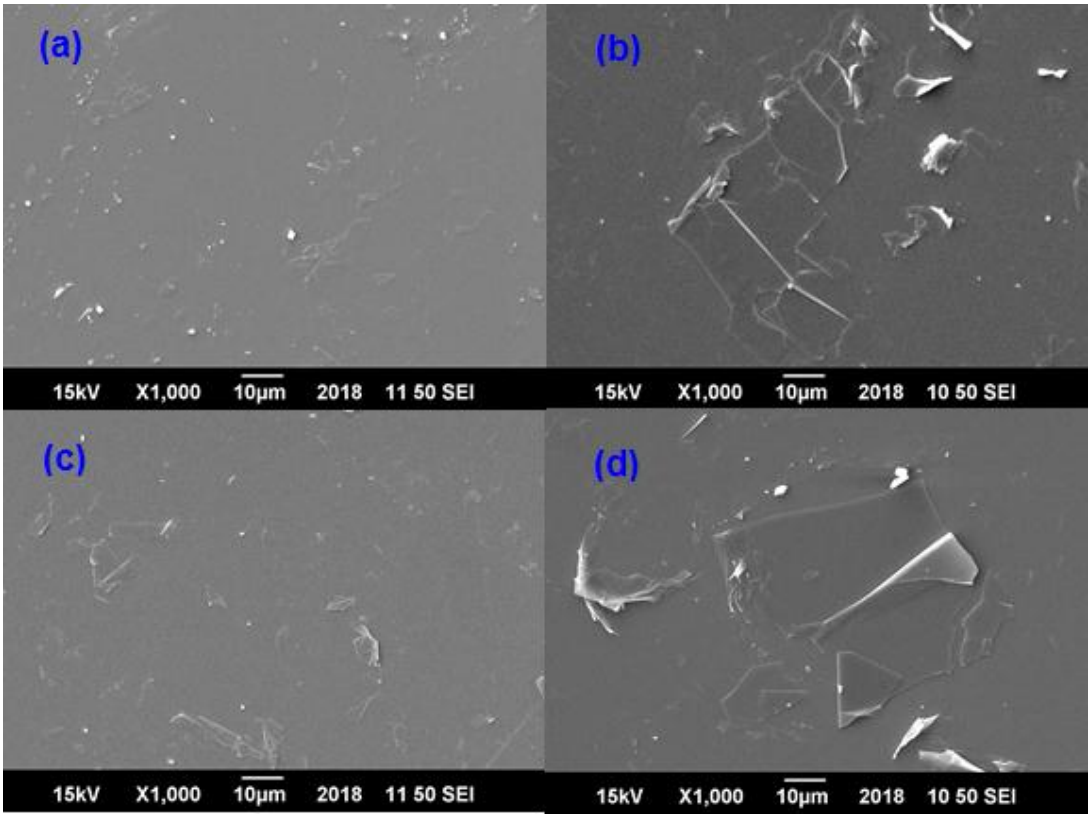

Figure 4.18: SEM images of (a) pristine graphene and MO doped graphene with different concentration (b) 2 X 10^{-7} M (c) 2 X 10^{-5} (d) 2 X 10^{-3} M at 1000X magnification

The doping was also analyzed by EDX as shown in Fig 4.19 below. EDX analysis Fig 4.19 (a, d) of pristine and Methyl Orange doped graphene flakes with different concentrations (b, f) 2 x 10^{-7} M (c, g) 2 x 10^{-5} (d, h) 2 x 10^{-3} M was reported. The improvement of carbon percentage for pristine and doped with MO (with increasing MO concentration) was confirmation that doping has been achieved.

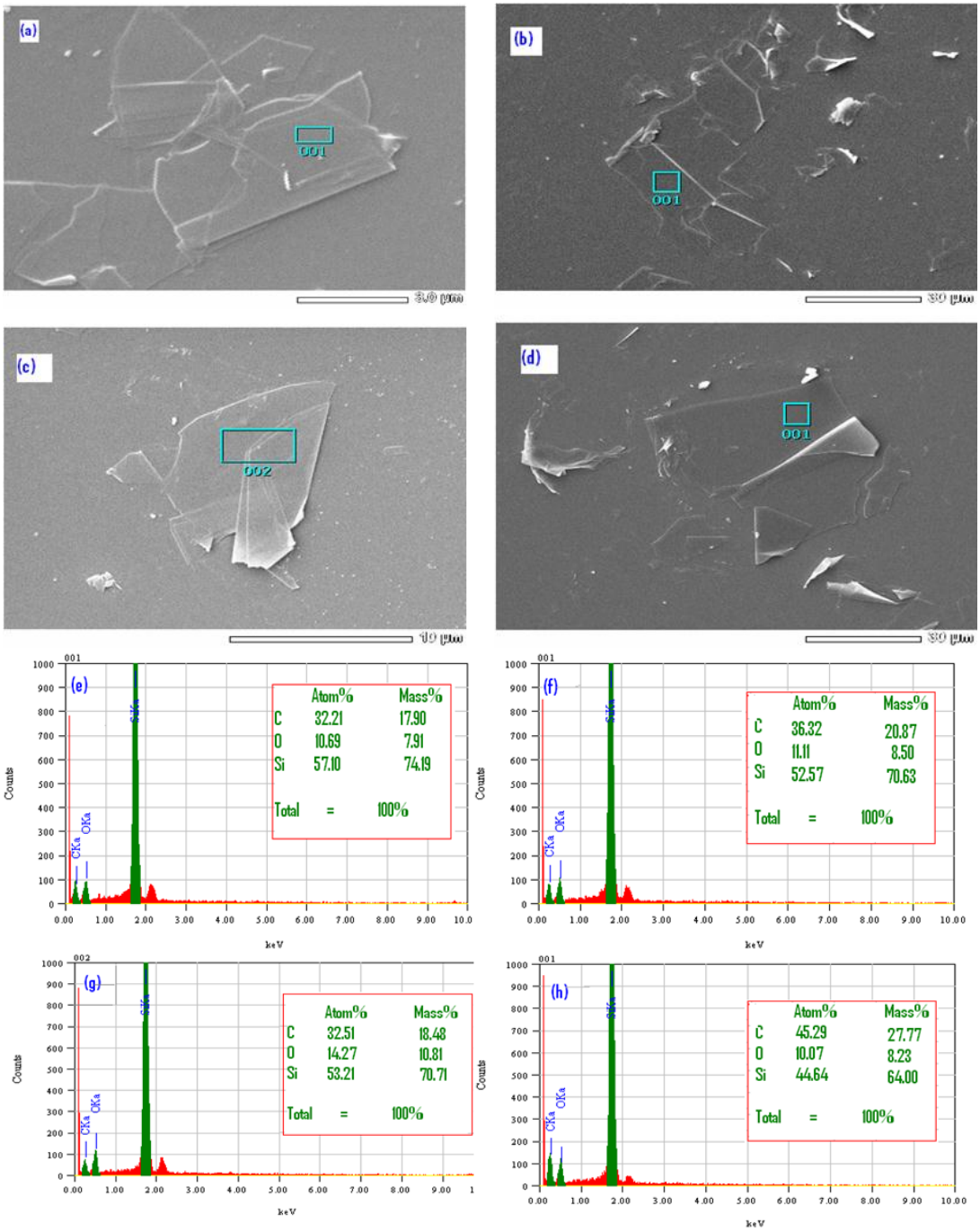

Figure 4.19: EDX analysis of (a, d) un-doped and Methyl Orange doped graphene flakes with different concentrations (b, f) 2 x 10^{-7} M (c, g) 2 x 10^{-5} (d, h) 2 x 10^{-3} M

4.4.1- (a): Doping of mono and few layers graphene and study of doping effects

Raman spectroscopy has been used for study of doping effect in mono and few layer graphene. The G band intensity and 2D band width has been the tool for determining number of graphene layers. Pure graphene sheets of all thickness produce G band peak at 1580 cm^{-1} and is finger print of graphene and graphite. The G band shows positive or negative shift with increasing thickness of graphene layers. However the shift decreases with increasing number of graphene layers. 2D spectrum of graphene comes near 2670 cm^{-1} and its width and position varies with thickness of graphene sheets. The shift of 2D band also has been reported. In addition with G and 2D band shift, very small peaks at 1158 cm^{-1}, 1290 cm^{-1} and 1500 cm^{-1} appear in mono layer graphene. This is confirmation of strong doping effect in mono layer graphene and this effect is decreased as graphene number of graphene layers increases.

Dopant species:

Methyl orange ($C_{14}H_{14}N_3NaO_3S$)

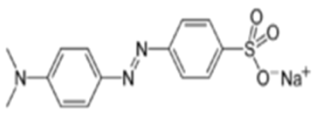

Sudan IV ($C_{24}H_{20}N_4O$)

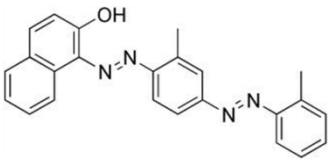

Fig 4.20 shows Raman spectra of mono, bi, tri and tetra layer graphene after molecular modification with methyl orange. The intensity ratios of G and 2D band, shape of 2D band and Raman shift in G band after molecular modification can identify the number of graphene layers. In Fig 4.20 (a), the intensity ratio I_{2D}/I_G is greater than two (2.18) and Raman shift in G band to 1588.81cm^{-1} identify the mono-layer graphene sheet. Similarly the Fig 4.20 (b) shows the I_{2D}/I_G ratio of graphene sheet is 0.93 (almost 1) and also the Raman shift in G band is 1584.2cm^{-1} which is confirmation of bi-layer graphene sheet. The shift in G band for Fig 4.20 (c) is nearly to 1583.1cm^{-1} and the intensity ratio I_{2D}/I_G is nearly about 0.76 which reflects the existence of tri-layer graphene. However, the Raman shift in G band for tetra-layer graphene is observed to be very small (1581.54cm^{-1}) and intensity ratio I_{2D}/I_G observed is nearly about 0.53, as shown in Fig 4.20 (c). Along with the blue shift in

G band (from 1580cm^{-1} for all pristine graphene), 2D band also shows blue shift after molecular modification with methyl orange. The blue shift in both G band and 2D band is confirmation of P-type doping effect caused by methyl orange in graphene layers. We can also observe that the Raman shift in G band for mono layer is more than the bi-layer and this shift decreases as the number of layer increases. The observed shifts are about 8.81cm^{-1}, 4.2cm^{-1}, 3.1cm^{-1} and 1.54cm^{-1} for mono, bi, tri and tetra-layer graphenes respectively as shown in Fig 4.22 (d). This means that doping effect in mono-layer > bi-layer > tri-layer > tetra layer. We can say that doping effect in graphene is layer dependent.

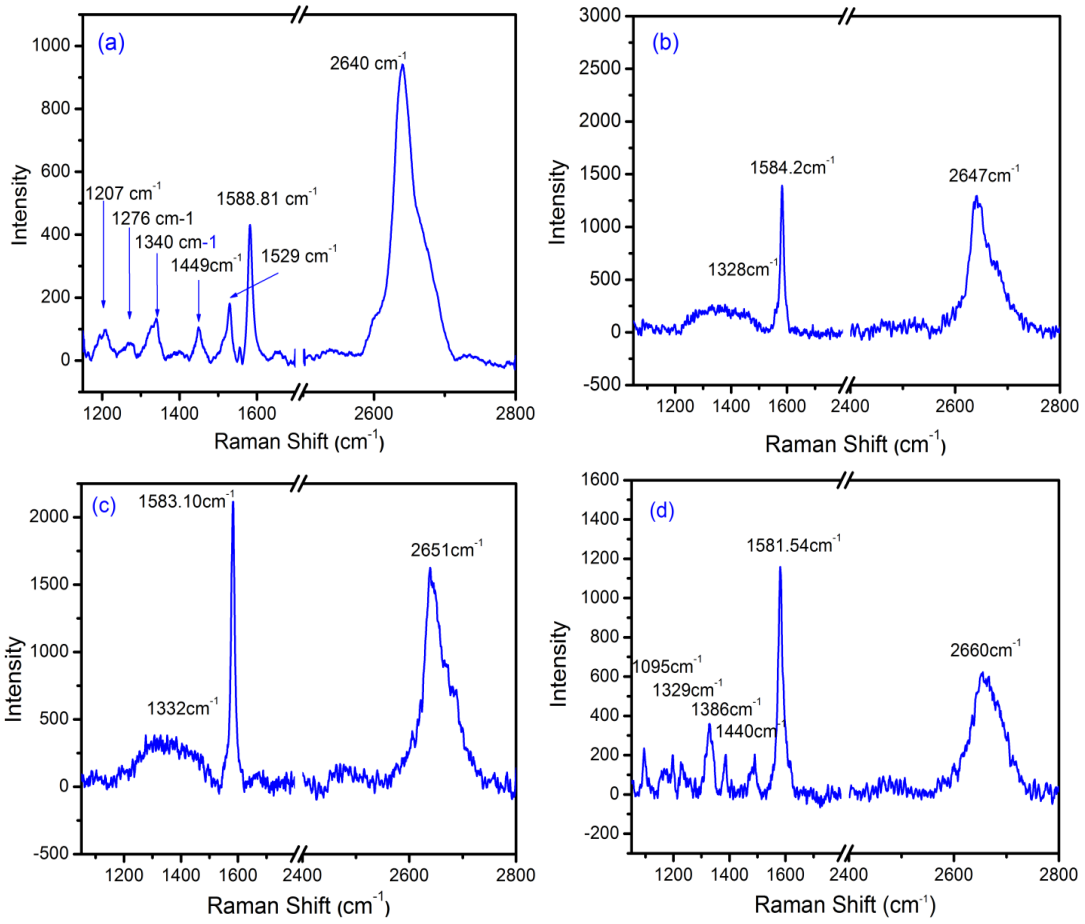

Fig 4.20: Raman spectra for methyl orange doped graphene, 1L (a), 2L (b), 3L (c) and 4L (d).

On doping, numerous MO bands are appeared between 1150 and 1550 cm^{-1} as shown in Fig 4.20 (a). The disorder related band (known as D band) is observed at 1340 cm^{-1}, which indicates that the disorders in the basal plane of graphene increases due to the dopant molecules. The small band observed at 1207 cm^{-1} is ascribed to the

stretching mode of C–S or C–C, the weak peak at 1290 cm^{-1} is ascribed to the stretching mode of C–N and the most intense band at 1529 cm^{-1} is originated from the stretching mode of N-aromatic ring.

The existence of the intense band at 1529cm^{-1} indicates that the parallel configuration of molecule on the surface of graphene sheet is promising. From the Raman spectroscopic analysis it is clear that the MO molecules are adsorbed on the surface of graphenes by π–π interaction.

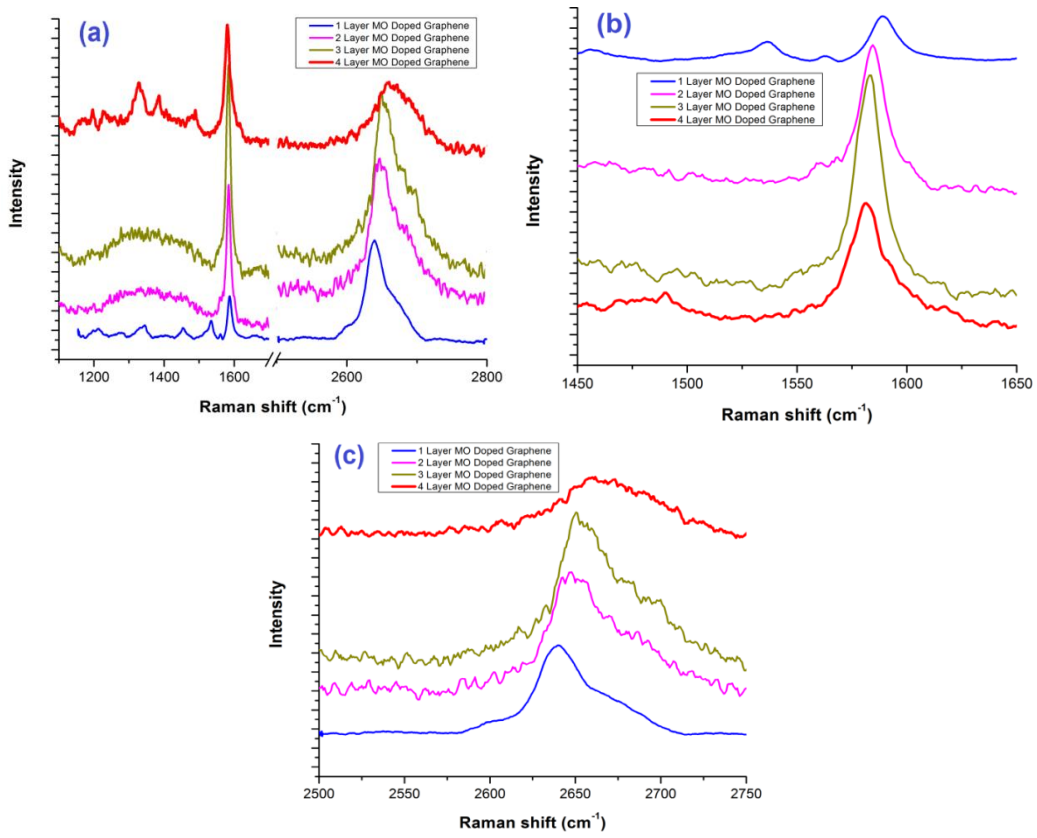

Fig 4.21: Relative intensity Raman Spectra of methyl orang doped different layer graphenes (a), relative shift in G band (b), and 2D band (c).

The Fig 4.21 (a) shows the relative intensities of all four layer graphene sheets and the Fig 4.21 (b) and (c) show the relative shift in G and 2D bands of mono to tetra-layer graphene sheets. The Raman shift in G band for mono layer is higher compared to few layer graphene as shown in Fig 4.21 (b). The 2D band position is lower compared to few layer graphene but it is observable that the pristine single layer and thicker graphene also give blue shift in their position without doping but after

molecular doping they may further give blue shift or red shift depending on the dopent species.

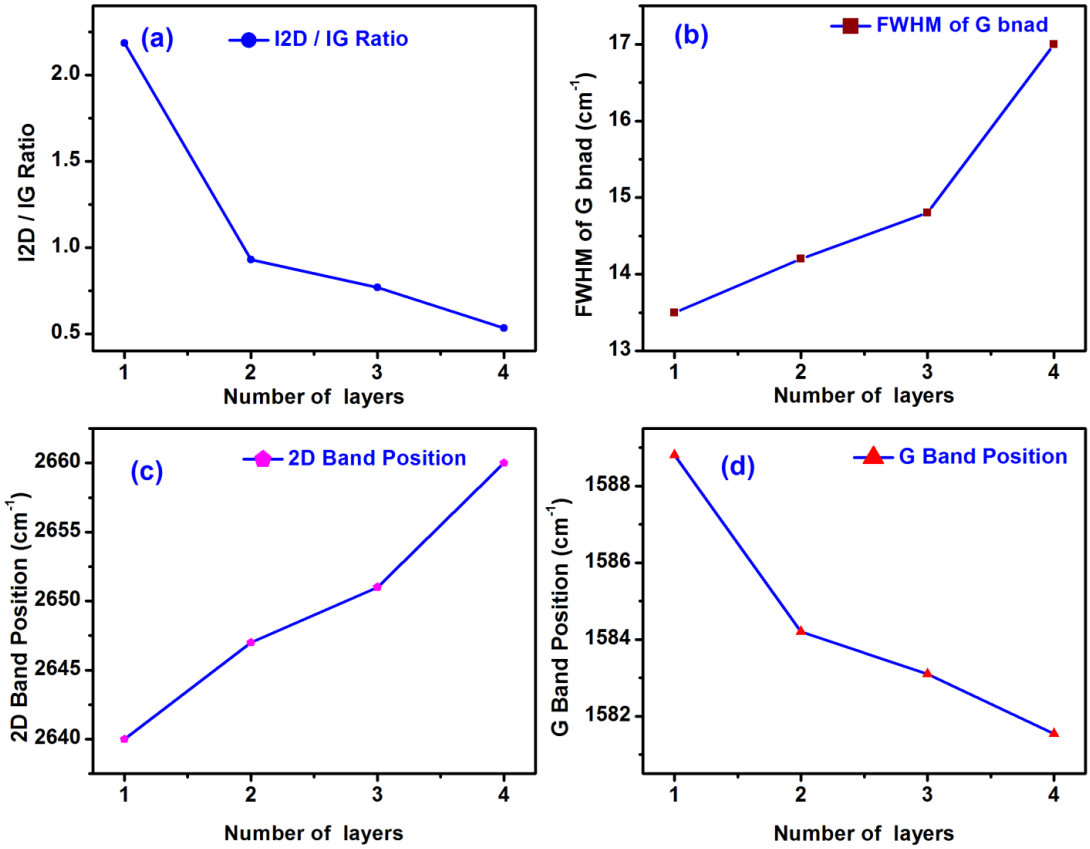

Fig 4.22: Statistical data for I2D/ IG ratios (a), FWHM of G band (b), 2D band position (c) and G band position (d) of few layer graphene after molecular modification with MO.

Fig 4.22 (a) shows the statistical data of intensity ratio I_{2D}/I_G of mono and few layer MO doped graphene. This ratio is large in mono layer graphene and as the number of layer increases the intensity ratio decreases. However by moving from mono to few layer graphene, the fall in ratio is large in the beginning (2.18 to 0.93 for mono to bi-layer) and it becomes relatively small (0.77 to 0.53 for tri to tetra-layer) for thick layer graphenes. The G band position for pristine mono and thick layer graphene is nearly at 1580cm^{-1} which is finger print of graphene and graphite. However, the Fig 4.22 (d) shows the statistical data for Raman shift in G band for mono and few layer graphene after molecular modification by methyl orange. The shift for mono layer graphene is highest up to about 8.81cm^{-1} and as the number of layer increases the

shift in G band decreases (up to 1.81cm^{-1} for tetra layer MO doped graphene). This is confirmation of strong molecular doping effect observed in mono layer graphene and this effect decreases as number of graphene layer increases.

Full width at half maximum (FWHM) for pristine mono and few layer graphenes is almost similar (~21cm^{-1}). The Fig 4.22 (b) shows the FWHM of G band for mono and few layer graphene after molecular modification. Its value is 13.5, 14.2, 14.8 and 17.0 cm^{-1} for mono, bi, tri and tetra-layer doped graphene. We can conclude that (i) FWHM doped/modified mono and few layer graphenes are always lower than the pristine graphenes and (ii) for mono layer modified graphene, the FWHM is lowest and as the number of layers of modified graphene increases, its value increases towards FWHM of Pristine graphenes (~21cm^{-1}). The Fig 4.22 (c) shows the statistical data for 2D band position of mono and few layer graphene and we can observe that 2D band position is lowest and it increases as the number of layer increases.

4.4.2- (b): Surface-enhanced Raman scattering (SERS) of Sudan Red IV on graphene substrate

Sudan IV (similar as Sudan I, II, and III) is very popular and common synthetic dye used in industry as color additive in different kind of foods, oils, solvent etc. However, if it is used for long period of time, it can cause cancer. According to the regulations related to Food Colorants, Cosmetics and Disinfectants etc., these colorants are strictly prohibited to be used. However, still it has been used by some manufacturers as color additive. Therefore, it is important and mandatory to find some effective and expedient techniques for the detection of such kind of color additives in routine usage goods.

Only a few methods for the measurement of Sudan Red have been reported so far. For the detection of such compounds in China and other countries, "High Performance Liquid Chromatography (HPLC) and Gas Chromatography-Mass Spectroscopy (GC-MS)" has been used [136]. However in case of HPLC, the detection of liquid chromatograph is difficult due to complex components of the chili oil, flavoring and many other foodstuffs mixed together. On the other hand GC-MS has problem of separation and multiple-purification of above described components.

Surface-enhanced Raman scattering (SERS), whose working principle is based on interaction of photons, has numerous advantages such as non-damage to samples and in situ detection with high-sensitivity and high-resolution. Since it has been employed to probe molecular structures, quick progress has been achieved for the matters identification, in many research fields. We have employed SERS to experience the interaction of photon with Sudan IV molecules and to examine its structure and atomic vibrational modes. We have used few-layer graphene (FLG) as SERS substrate for the trace quantity detection of Sudan IV compound for the first time.

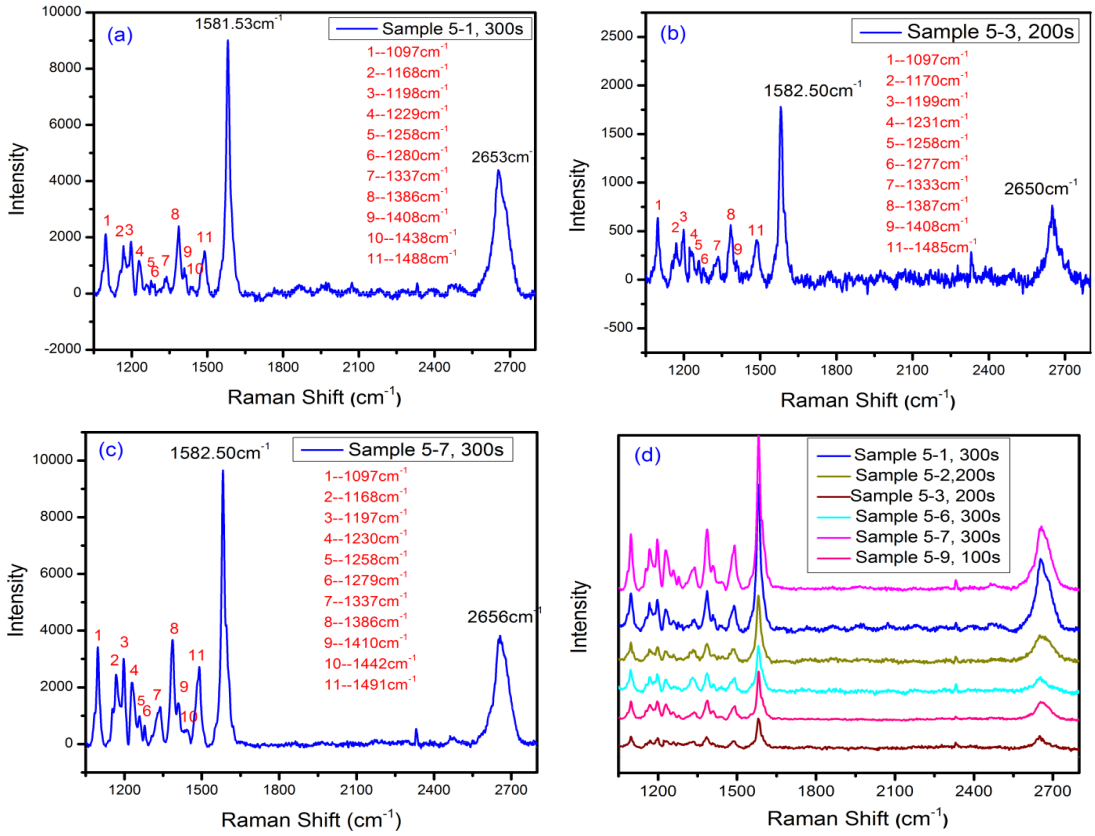

Figure 4.23: SERS spectra of Sudan IV molecules on FLG sheets with different number of graphene layers (a-c) and relative intensity & position of Sudan IV signals on FLG sheets (d).

In our current work, $2x10^{-5}$ M solution of Sudan IV was spin coated on few layer graphene sheets mounted on the Si/SiO_2 substrate by adhesive tap method. Raman and SERS spectra for Sudan IV have been taken at the surface of few layer graphene

sheets as well as on the surface of naked Si/SiO_2 where there exists no graphene sheet. We observed no signals/peaks for Sudan IV on naked Si/SiO_2 surface, whereas very strong signals/peaks were clearly observed for Sudan IV on the surface of few layer graphene sheets as shown in Fig.4.23.

Fig 4.23 shows SERS spectra of Sudan IV on few-layer graphene (FLG) sheets with different number of layers Fig 4.23 (a-c) and relative intensity and position of SERS peaks at different FLG sheets Fig 4.23 (d). The SERS spectra taken from different FLG sheets contain peaks at similar positions and almost have similar intensities. The most intense peaks observed in SERS spectra at 1097, 1230, 1386 and 1491cm^{-1} were as a result of vibrational modes of atoms and bonds of Sudan IV molecules, as shown in Table 3. Therefore from experimental results it is obviously clear that we have obtained more reasonable and reliable method for the recognition and analysis of trace quantity Sudan IV molecules.

Table 3: Assignment of vibrational modes for Sudan Red IV molecules SERS signals

Peaks (cm^{-1})	1097(s)	1168(m)	1197(s), 1230(s)	1258(w), 1279(w)	1337(m)	1386(s)	1410(w), 1442(w), 1491(s)
Assignment	v_2(CC) and v(CN)	v_{12}(CC)	β(C-H) and β(OH)	In-plane ring and β(OH)	β(C-H)	v(CN) & V_{12}(CC)	Ring dilation vibration

Note: w: weak; m: medium; s: strong

4.5- To induce band gap in few layer graphene by doping

UV/Vis spectroscopy was used to calculate the band gap of pristine and methyl orange doped graphene. The doping was done by methyl orange solution in three different concentrations $2x10^{-7}$ M, $2x10^{-5}$ M, and $2x10^{-3}$ M. The observed band gaps were 1.490 eV, 1.5570 eV, 1.6249 eV & 1.8718 eV for pristine graphene, $2x10^{-7}$ M, $2x10^{-5}$ M, and $2x10^{-3}$ M methyl orange (MO) doped graphene respectively. However the pure graphene has zero band gap. The possible reason could be as samples were prepared by Adhesive tap method which left glue residue creating this error. To minimize this effect we took this band gap as zero and subtract this factor from all calculated band gaps of doped graphene. Thus the corrected observed band gap

found were about 0.088eV, 0.1559eV and 0.4028eV for 2 x 10^{-7} M, 2 x 10^{-5} M and 2 x 10^{-3} M MO-doped graphene respectively.

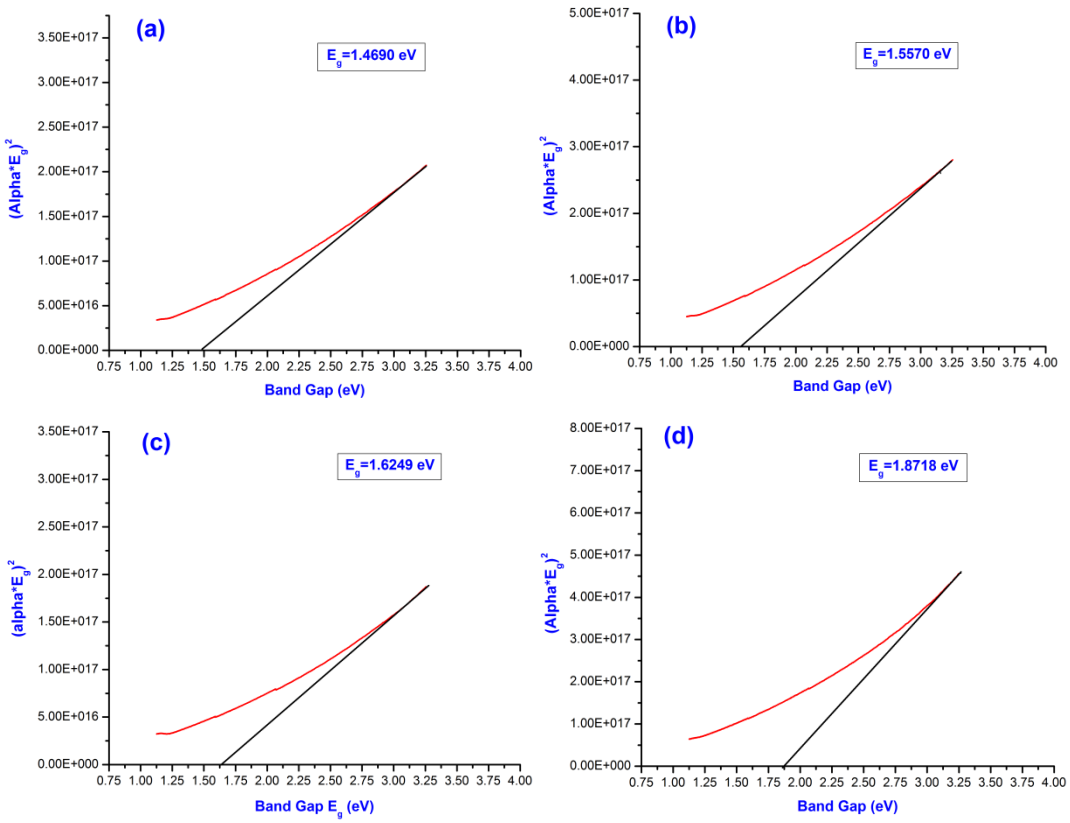

Figure 4.24: Band gap of (a) un-doped and MO doped graphene with (b) 2x10^{-7} M (c) 2x10^{-5} M and (d) 2x10^{-3} M concentrations.

Conclusion

Graphene! a two dimensional material has been considered the most hot research topic since it was successfully isolated for the first time due to its unique mechanical, electrical, optical and thermal properties. In our work, we have concentrated on doping and characterization of mono and few-layer graphene (MFLG) with methyl orange (MO) and Sudan IV. Furthermore, we have doped graphene to induce band gap for semiconducting uses and also used graphene as SERS substrate for the detection of trace quantity of Sudan IV.

The numbers of graphene layer are identified by using three different approaches optical microscopy, AFM and Raman Spectroscopy on oxidized silicon substrate. Different graphene sheets produced different color contrasts with SiO_2 layer of 300 nm thickness on Si/SiO_2 substrate, due to interference phenomenon. The light purple color sheet in our case is mono layer graphene and the color becomes dark purple as the number of layer increases. The optical microscopic identification based on color contrast between and oxidized silicon surface gave a rough idea about the number of layers in graphene sheets. To do accurate identification of graphene thickness, we performed AFM measurement by using step height difference of scanning line. However, Raman Spectroscopy gave true identification of graphene layers by using I_{2D}/I_G ratio and G band shift after doping with MO. The surface morphology of FLG was analyzed by AFM, SEM and STM which shows that transparent, smooth and very less defect containing graphene sheets. Furthermore EDX analysis was performed for elemental composition on surface of FLG sheets before and after modification with MO with different concentrations.

The study of thickness dependent doping effect is carried out by modifying MFLG sheets with MO molecules. The doping effect is characterized by Raman spectroscopy. The Raman spectroscopy analysis of doped graphene shows blue shift in G band and this shift is largest in mono layer graphene and decreased as the number of graphene layer increases. This means doping effect is thickness dependent and it is strong in mono layer graphene but decreases as the number of graphene layers increases. We can conclude that doping effect in mono-layer > bi-layer > tri-layer > tetra layer.

The Sudan Red molecules can cause cancer in human body if taken in large quantity and are strictly forbidden by the “International Agency for Research on Cancer”. We

used Surface-enhanced Raman Scattering (SERS) technique for the identification of Sudan Red IV compound. Importantly, we realized a new method for identification of trace quantity Sudan IV molecules using graphene as SERS substrate for the first time. This method can be used as the economical and convenient method for detection of Sudan IV molecules and other such strictly forbidden colorants for the prevention of their usage in Food Colorants, Cosmetics and Disinfectants.

The pristine graphene is a zero band gap conductor. To induced band gap in FLG, we doped it with MO dye containing electron withdrawing functional groups, with different concentrations. The induced band gap is characterized by UV/Vis Spectroscopy. The UV/Vis spectroscopy analysis showed a 0.40eV increase in band gape of MO doped graphene. Furthermore, doping effect and increase in band gap are concentration dependent as well.

Suggestions

Further research is desirable for the detection of Sudan Red Molecules by using graphene as SERS substrate which can help to improve the new detection technique for Sudan Red molecules.

Chapter 5 References

1. A. H. Castro Neto, F.G., and N. M. R. Peres, Physics World, November 2006.
2. Slonczewski, J.C. and P.R. Weiss, *Band Structure of Graphite.* Physical Review, 1958. **109**(2): p. 272-279.
3. Zhang, Y., et al., *Experimental observation of the quantum Hall effect and Berry's phase in graphene.* Nature, 2005. **438**(7065): p. 201-4.
4. Novoselov, K.S., et al., *Room-temperature quantum Hall effect in graphene.* science, 2007. **315**(5817): p. 1379.
5. Novoselov, K.S., et al., *Two-dimensional gas of massless Dirac fermions in graphene.* Nature, 2005. **438**(7065): p. 197-200.
6. Novoselov, K.S., et al., *Electric field effect in atomically thin carbon films.* science, 2004. **306**(5696): p. 666-9.
7. Balandin, A.A., et al., *Superior thermal conductivity of single-layer graphene.* Nano Lett, 2008. **8**(3): p. 902-7.
8. Lee, C., et al., *Measurement of the elastic properties and intrinsic strength of monolayer graphene.* science, 2008. **321**(5887): p. 385-8.
9. Wu J, B.H., Bao Z, Liu Z, Chen Y, Peumans P, *Organic solar cells with solution-processed graphene transparent electrodes.* Appl Phys Lett 2008. **92**.
10. Li, X., et al., *Chemically derived, ultrasmooth graphene nanoribbon semiconductors.* science, 2008. **319**(5867): p. 1229-32.
11. Ritter, K.A. and J.W. Lyding, *The influence of edge structure on the electronic properties of graphene quantum dots and nanoribbons.* Nat Mater, 2009. **8**(3): p. 235-42.
12. Ubbelohde AR, L.L., *Graphite and its crystal compounds.* London: Oxford University Press, 1960.
13. Thompson TE, F.E., Hanlon LR, *The electrical conductivity and optical reflectance of graphite–SbF5 compounds.* carbon, 1977.
14. Fuzellier H, M.J., Herold A., *Conductibilité électrique des composés lamellaires graphite–SbF5 et graphite–SbCl5.* carbon, 1977. **15**.
15. Shenderova OA, Z.V., Brenner DW, *Carbon nanostructures.* Crit Rev Solid State Mater Sci 2002. **27**.
16. Krishnan A, D.E., Treacy MMJ, Hugdahl J, Lynum S, Ebbesen TW, *Graphitic cones and the nucleation of curved carbon surfaces.* nature, 1997. **388**.
17. Land TA, M.T., Behm RJ, Hemminger JC, Comsa G, *STM investigation of single layer graphite structures produced on Pt(111) by hydrocarbon decomposition.* surf sci, 1992. **264**.
18. Nagashima A, N.K., Itoh H, Ichinokawa T, Oshima C, Otani S, *Electronic states of monolayer graphite formed on TiC(111) surface.* surf sci, 1993. **291**.
19. Forbeaux I, T.J., Debever JM, *Heteroepitaxial graphite on 6H–SiC(0001): interface formation through conductionband electronic structure.* physical Review B, 1998. **58**.
20. Berger C, S.Z., Li TB, Li XB, Ogbazghi AY, Feng R, et al, *Ultrathin epitaxial graphite: 2D electron gas properties and a route toward graphene-based nanoelectronics.* J Phys Chem B 2004. **108**.

21. Berger, C., et al., *Electronic confinement and coherence in patterned epitaxial graphene.* science, 2006. **312**(5777): p. 1191-6.
22. Bolotin KI, S.K., Jiang Z, Klima M, Fudenberg G, Hone J, et al. , *Ultrahigh electron mobility in suspended graphene.* . Solid State Commun 2008. **146**.
23. Nair, R.R., et al., *Fine structure constant defines visual transparency of graphene.* science, 2008. **320**(5881): p. 1308.
24. Zhang YB, T.Y., Stormer HL, Kim P, *Experimental observation of the quantum Hall effect and Berry's phase in graphene.* Nature, 2005. **438**.
25. Novoselov, K.S., et al., *Two-dimensional atomic crystals.* Proc Natl Acad Sci U S A, 2005. **102**(30): p. 10451-3.
26. Oostinga, J.B., et al., *Gate-induced insulating state in bilayer graphene devices.* Nat Mater, 2008. **7**(2): p. 151-7.
27. Bae, S., et al., *Roll-to-roll production of 30-inch graphene films for transparent electrodes.* Nat Nanotechnol, 2010. **5**(8): p. 574-8.
28. Kravets VG, G.A., Nair RR, Blake P, Anissimova S, Novoselov KS, et al., *Spectroscopic ellipsometry of graphene and an exciton-shifted van Hove peak in absorption.* Phys Rev B 2010. **81**.
29. Park, S. and R.S. Ruoff, *Chemical methods for the production of graphenes.* Nat Nanotechnol, 2009. **4**(4): p. 217-24.
30. Elias, D.C., et al., *Control of graphene's properties by reversible hydrogenation: evidence for graphane.* science, 2009. **323**(5914): p. 610-3.
31. Bonaccorso F, S.Z., Hasan T, Ferrari AC, *Graphene photonics and optoelectronics.* Nat Photon 2010. **4**.
32. Gokus, T., et al., *Making graphene luminescent by oxygen plasma treatment.* ACS Nano, 2009. **3**(12): p. 3963-8.
33. Luo Z, V.P., Mele EJ, Johnson ATC, Kikkawa JM, *Photoluminescence and band gap modulation in graphene oxide.* Appl Phys Lett 2009. **94**.
34. Tsoukleri, G., et al., *Subjecting a graphene monolayer to tension and compression.* Small, 2009. **5**(21): p. 2397-402.
35. Lee C, W.X., Li QY, Carpick R, Kysar JW, Hone J. , *Elastic and frictional properties of graphene.* Phys Status Solidi B – Basic Solid State Phys 2009. **246**.
36. Yu T, N.Z., Du C, You Y, Wang Y, Shen Z., *Raman mapping investigation of graphene on transparent flexible substrate: the strain effect.* J Phys Chem C 2008. **112**.
37. Ni ZH, C.W., Fan XF, Kuo JL, Yu T, Wee ATS, et al., *Raman spectroscopy of epitaxial graphene on a SiC substrate.* Phys Rev B 2008. **77**.
38. Ni, Z.H., et al., *Tunable stress and controlled thickness modification in graphene by annealing.* ACS Nano, 2008. **2**(5): p. 1033-9.
39. Ni, Z.H., et al., *Uniaxial strain on graphene: Raman spectroscopy study and band-gap opening.* ACS Nano, 2008. **2**(11): p. 2301-5.
40. Mohiuddin TMG, L.A., Nair RR, Bonetti A, Savini G, Jalil R, et al, *Uniaxial strain in graphene by Raman spectroscopy: G peak splitting, Gruneisen parameters, and sample orientation.* Phys Rev B 2009. **79**.
41. C. H. Yu , L.S., Z. Yao , D. Y. Li , A. Majumda, Nano Lett, 2005. **5**.
42. S. Berber , Y.K.K., D. Tomanek ,, Phys. Rev. Lett, 2000. **84**.
43. D. L. Nika , E.P.P., A. S. Askerov , A. A. Balandin Phys. Rev. B, 2009. **79**.
44. Z. Guo , D.Z., X.-G. Gong, Appl. Phys. Lett, 2009. **95**.
45. A. A. Balandin , S.G., W. Z. Bao , I. Calizo , D. Teweldebrhan ,F. Miao , C. N. Lau Nano Lett, 2008. **8**.

46. S. Ghosh , I.C., D. Teweldebrhan , E. P. Pokatilov , D. L. Nika , A.A. Balandin , W. Bao , F. Miao , C. N. Lau, Appl. Phys. Lett. , 2008. **92**.
47. Hsu, I.K., et al., *Optical absorption and thermal transport of individual suspended carbon nanotube bundles.* Nano Lett, 2009. **9**(2): p. 590-4.
48. I. Calizo , A.A.B., W. Bao , F. Miao , C. N. Lau Nano Lett, 2007. **7**.
49. J. H. Seol , I.J., A. L. Moore , L. Lindsay , Z. H. Aitken , M. T. Pettes ,X. Li , Z. Yao , R. Huang , D. Broido , N. Mingo , R. S. Ruoff , L. Shi science, 2010. **328**.
50. W. Cai , A.L.M., Y. Zhu , X. Li , S. Chen , L. Shi , R. S. Ruoff Nano Lett, 2010. **10**.
51. Zhang YB, S.J., Pontius WV, Kim P, *Fabrication and electric-field-dependent transport measurements of mesoscopic graphite devices.* Appl Phys Lett 2005. **86(7)**.
52. Chen, J.H., et al., *Intrinsic and extrinsic performance limits of graphene devices on SiO2.* Nat Nanotechnol, 2008. **3**(4): p. 206-9.
53. Bolotin KI, S.K., Jiang Z, Klima M, Fudenberg G, Hone J, et al, *Ultrahigh electron mobility in suspended graphene.* Solid State Commun, 2008. **146**(9-10): p. 351-5.
54. Ishigami, M., et al., *Atomic structure of graphene on SiO2.* Nano Lett, 2007. **7**(6): p. 1643-8.
55. Moser J, B.A., Bachtold A, *Current-induced cleaning of graphene.* Appl Phys Lett 2007. **91**(16).
56. Hass J, H.W., Conrad EH, *The growth and morphology of epitaxial multilayer graphene.* J Phys: Condens Matter 2008. **20**.
57. de Heer WA, B.C., Wu X, First PN, Conrad EH, Li X, et al, *Epitaxial graphene.* Solid State Commun 2007. **143**.
58. Varchon, F., et al., *Electronic structure of epitaxial graphene layers on SiC: effect of the substrate.* Phys Rev Lett, 2007. **99**(12): p. 126805.
59. Penuelas J, O.A., Lucot D, David C, Gierak J, Estrade-Szwarckopt H, et al, *Surface morphology and characterization of thin graphene films on SiC vicinal substrate.* Phys Rev B 2009. **79**: p. 033408.
60. Tedesco JT, J.G., Culbertson JC, Hite JK, Yang Y, Daniels KM, et al, *Morphology characterization of argon-mediated epitaxial graphene on C-face SiC.* Appl Phys Lett 2010. **96**: p. 222103.
61. Emtsev, K.V., et al., *Towards wafer-size graphene layers by atmospheric pressure graphitization of silicon carbide.* Nat Mater, 2009. **8**(3): p. 203-7.
62. Cassell AM, R.J., Kong J, Dai HJ, *Large scale CVD synthesis of single-walled carbon nanotubes.* J Phys Chem B 1999. **1033**(31): p. 6484-92.
63. Talapatra, S., et al., *Direct growth of aligned carbon nanotubes on bulk metals.* Nat Nanotechnol, 2006. **1**(2): p. 112-6.
64. Fujita TKW, O.C., *Novel structures of carbon layers on a Pt(1 1 1) surface.* Surf Interface Anal 2005. **37**(2): p. 120-3.
65. A.M. Affoune, B.L.V.P., H. Sato, T. Enoki, Y. Kaburagi, Y. Hishiyama, Chem. Phys. Lett, 2001. **348**: p. 17.
66. C. Berger, Z.S., X. Li, X. Wu, N. Brown, C. Naud, D. Mayou, T. Li, J. Hass, A.N. Marchenkov, E.H. Conrad, P.N. First, W.A, science, 2006. **312**.
67. A. Reina, X.J., J. Ho, D. Nezich, H. Son, V. Bulovic, M.S. Dresselhaus, J. Kong, Nano Lett, 2009. **9**.
68. Liu, W., et al., *Synthesis of high-quality monolayer and bilayer graphene on copper using chemical vapor deposition.* carbon, 2011. **49**(13): p. 4122-4130.

69. Gautam, M. and A.H. Jayatissa, *Gas sensing properties of graphene synthesized by chemical vapor deposition.* Materials Science & Engineering C-Materials for Biological Applications, 2011. **31**(7): p. 1405-1411.
70. Ding, X.L., et al., *Direct growth of few layer graphene on hexagonal boron nitride by chemical vapor deposition.* carbon, 2011. **49**(7): p. 2522-2525.
71. Park, H.J., et al., *Growth and properties of few-layer graphene prepared by chemical vapor deposition.* carbon, 2010. **48**(4): p. 1088-1094.
72. Chung, D.D.L., J. Mater. Sci, 1987. **22**.
73. Inagaki, M., J. Mater. Res, 1989. **4**.
74. R. A. Greinke, R.A.M., and E. J. Beck, U.S. Patent No, 1990. **4895713**.
75. G. H. Chen, D.J.W., W. U. Weng, and C. L. Wu, C A R B ON, 2003. **41**.
76. G. H. Chen, W.G.W., D. J. Wu, C. L. Wu, J. R. Lu, P. P. Wang, and X. F. Chen, C A R B ON, 2004. **42**.
77. X. H. Chen, H.S.Y., G. T. Wu, M. Wang, F. M. Deng, X. B. Zhang, J. C. Peng, and W. Z. Li, J. Cryst. Growth 2000. **218**.
78. L. M. Viculis, J.J.M., O. M. Mayer, H. T. Hahn, and R. B. Kaner,, J. Mater. Chem, 2005. **15**.
79. X. L. Li, X.R.W., L. Zhang, S. W. Lee, and H. J. Dai, science, 2008. **319**.
80. B. C. Brodie, P., R. Soc. London 1859. **149**.
81. Hummers, W.S. and R.E. Offeman, *Preparation of Graphitic Oxide.* Journal of the American Chemical Society, 1958. **80**(6): p. 1339-1339.
82. Z. S. Wu, W.C.R., L. B. Gao, J. P. Zhao, Z. P. Chen, B. L. Liu, D. M. and B.Y. Tang, C. B. Jiang, and H. M. Cheng, ACS Nano 2009. **3**.
83. S. Horiuchi, T.G., M. Fujiwara, T. Asaka, T. Yokosawa, and Y. Matsui, Appl. Phys. Lett, 2004. **84**.
84. S. Horiuchi, T.G., M. Fuijwara, R. Sotoaka, M. Hirata, K. Kimoto, T. Asaka, T. Yokosawa, Y. Matsui, K. Watanabe, and M. Sekita,, Jpn. J. Appl. Phys, 2003. **42**.
85. A. G. Cano-M´arquez, F.J.R.ı.-M.ı., J. Campos- Delgado, C. G. Espinosa-Gonz´alez, F. Trist´an-L´opez, D. Ram´ıre- Gonz´alez, D. A. Cullen, et al, *Ex-MWNTs: graphene sheets and ribbons produced by lithium intercalation and exfoliation of carbon nanotubes,.* Nano Lett, 2009. **9**.
86. L. Jiao, L.Z., X. Wang, G. Diankov, and H. Dai,, *Narrow graphene nanoribbons from carbon nanotubes.* Nature, 2009. **458**.
87. C.-D. Kim, B.-K.M., and W.-S. Jung,, *Preparation of graphene sheets by the reduction of carbon monoxide.* C A R B ON, 2009. **47**: p. 1610.
88. D. V. Kosynkin, A.L.H., A. Sinitskii, J. R. Lomeda, A. Dimiev, B. K. Price, and J. M. Tour, *Longitudinal unzipping of carbon nanotubes to form graphene nanoribbons.* Nature, 2009. **458**.
89. Y. Zhang, J.P.S., W. V. Pontius, and P. Kim, *Fabrication and electric-field-dependent transport measurements of mesoscopic graphite devices.* Appl Phys Lett, 2005. **86**.
90. Das A, P.S., Chakraborty B, Piscanec S, Saha SK, Waghmare UV, et al., Nat Nanotechnol 2008. **3**.
91. Zhang YB, T.T., Girit C, Hao Z, Martin MC, Zettl A, et al, Nature, 2009. **459**.
92. Santos JE, P.N., dos Santos J, Neto AHC, Phys Rev B 2011. **84**.
93. Miwa RH, S.T., Scopel WL, Fazzio A. , Appl Phys Lett 2011. **99**.
94. Zhao, L., et al., *Visualizing individual nitrogen dopants in monolayer graphene.* science, 2011. **333**(6045): p. 999-1003.

95. Yu, W.J., et al., *Toward tunable band gap and tunable dirac point in bilayer graphene with molecular doping.* Nano Lett, 2011. **11**(11): p. 4759-63.
96. Giovannetti, G., et al., *Doping graphene with metal contacts.* Phys Rev Lett, 2008. **101**(2): p. 026803.
97. Ling, X., et al., *Can graphene be used as a substrate for Raman enhancement?* Nano Lett, 2010. **10**(2): p. 553-61.
98. Panchokarla, L.S., et al., *Synthesis, Structure, and Properties of Boron- and Nitrogen-Doped Graphene.* Advanced Materials, 2009. **21**(46): p. 4726-+.
99. Dai, J.Y., J.M. Yuan, and P. Giannozzi, *Gas adsorption on graphene doped with B, N, Al, and S: A theoretical study.* Applied Physics Letters, 2009. **95**(23).
100. Zou, Y., et al., *An ab initio study on gas sensing properties of graphene and Si-doped graphene.* European Physical Journal B, 2011. **81**(4): p. 475-479.
101. Zhou, S.Y., et al., *Metal to insulator transition in epitaxial graphene induced by molecular doping.* Physical Review Letters, 2008. **101**(8).
102. Wehling, T.O., et al., *Molecular doping of graphene.* Nano Lett, 2008. **8**(1): p. 173-7.
103. Kasry, A., et al., *Chemical doping of large-area stacked graphene films for use as transparent, conducting electrodes.* ACS Nano, 2010. **4**(7): p. 3839-44.
104. Kaverzin, A.A., et al., *Electrochemical doping of graphene with toluene.* carbon, 2011. **49**(12): p. 3829-3834.
105. Lherbier, A., et al., *Charge transport in chemically doped 2D graphene.* Physical Review Letters, 2008. **101**(3).
106. Wei, D.C., et al., *Synthesis of N-Doped Graphene by Chemical Vapor Deposition and Its Electrical Properties.* Nano Lett, 2009. **9**(5): p. 1752-1758.
107. Jin, Z., et al., *Large-Scale Growth and Characterizations of Nitrogen-Doped Monolayer Graphene Sheets.* ACS Nano, 2011. **5**(5): p. 4112-4117.
108. Guo, B.D., et al., *Controllable N-Doping of Graphene.* Nano Lett, 2010. **10**(12): p. 4975-4980.
109. Reina, A., et al., *Large Area, Few-Layer Graphene Films on Arbitrary Substrates by Chemical Vapor Deposition.* Nano Lett, 2009. **9**(1): p. 30-35.
110. Li, X.S., et al., *Large-Area Synthesis of High-Quality and Uniform Graphene Films on Copper Foils.* science, 2009. **324**(5932): p. 1312-1314.
111. Gomez-Navarro, C., et al., *Electronic transport properties of individual chemically reduced graphene oxide sheets.* Nano Lett, 2007. **7**(11): p. 3499-3503.
112. Garcia AG, B.S., Castro AHR, Robles JFP, Rubio A. , J Comput Theor Nanosci, 2008. **5**.
113. Lu, X.J., et al., *Low-temperature rapid synthesis of high-quality pristine or boron-doped graphene via Wurtz-type reductive coupling reaction.* Journal of Materials Chemistry, 2011. **21**(29): p. 10685-10689.
114. Lin, T.Q., et al., *A facile preparation route for boron-doped graphene, and its CdTe solar cell application.* Energy & Environmental Science, 2011. **4**(3): p. 862-865.
115. Denis, P.A., R. Faccio, and A.W. Mombru, *Is it possible to dope single-walled carbon nanotubes and graphene with sulfur?* Chemphyschem, 2009. **10**(4): p. 715-22.

116. Medina, H., et al., *Tuning of Charge Densities in Graphene by Molecule Doping.* Advanced Functional Materials, 2011. **21**(14): p. 2687-2692.
117. Zhang, W.J., et al., *Opening an Electrical Band Gap of Bilayer Graphene with Molecular Doping.* ACS Nano, 2011. **5**(9): p. 7517-7524.
118. BT, K., *Physics of graphite.* London: Applied Science Publishers, 1981.
119. Jung I, P.M., Piner R, Dikin DA, Stankovich S, Watcharotone S, et al, *Simple approach for high-contrast optical imaging and characterization of graphene-based sheets.* Nano Lett, 2007. **7**.
120. Lambacher A, F.P., *Fluorescence interference-contrast microscopy on oxidized silicon using a monomolecular dye layer.* Appl Phys A – Mater Sci Process 1996. **63**.
121. Ni ZH, W.H., Kasim J, Fan HM, Yu T, Wu YH, et al. , *Graphene thickness determination using reflection and contrast spectroscopy.* Nano Lett, 2007. **7**.
122. L, W., *The optical constants of bulk materials and films.* Institute of Physics, 1994.
123. Park JS, R.A., Saito R, Kong J, Dresselhaus G, Dresselhaus MS, *G' band Raman spectra of single, double and triple layer graphene.* C A R B ON, 2009. **47**.
124. Paredes, J.I., et al., *Atomic force and scanning tunneling microscopy imaging of graphene nanosheets derived from graphite oxide.* Langmuir, 2009. **25**(10): p. 5957-68.
125. Hashimoto A, S.K., Gloter A, Urita K, Iijima S, *Direct evidence for atomic defects in graphene layers.* Nature, 2002. **430**.
126. Meyer, J.C., et al., *The structure of suspended graphene sheets.* Nature, 2007. **446**(7131): p. 60-3.
127. Meyer JC, G.A., Katsnelson MI, Novoselov KS, Obergfell D, Roth S, et al, *On the roughness of single- and bi-layer graphene membranes.* Solid State Commun 2007. **143**(1-2).
128. Liu, Z., et al., *Open and closed edges of graphene layers.* Phys Rev Lett, 2009. **102**(1): p. 015501.
129. Meyer, J.C., et al., *Direct imaging of lattice atoms and topological defects in graphene membranes.* Nano Lett, 2008. **8**(11): p. 3582-6.
130. GoÌmez-Navarro C, M.J., Sundaram RS, Chuvilin A, Kurasch S, Burghard M, et al., *Atomic structure of reduced graphene oxide.* Nano Lett, 2010. **10**.
131. Girit CO, M.J., Erni R, Rossell MD, Kisielowski C, Yang L, et al, *Graphene at the edge: stability and dynamics.* science, 2009. **323**.
132. Ferrari, A.C., et al., *Raman spectrum of graphene and graphene layers.* Phys Rev Lett, 2006. **97**(18): p. 187401.
133. L. Malard, M.A.P., G. Dresselhaus, M.S. Dresselhaus, Phys. Rep, 2009. **473**.
134. Z. H. Ni, H.M.W., J. Kasim, H. M. Fan, *Graphene Thickness Determination Using Reflection and Contrast Spectroscopy.* Nano Lett, 2007. **7**(9): p. 2758-2763.
135. A. Gupta, G.C., P. Joshi, *Raman Scattering from High Frequency Phonons in Supported n-Graphene Layer Films.* Nano Lett, 2006. **6**(12).
136. Zhou Xiaofang, Y.F.a.P.X.Z., *Experimental and Theoretical Analysis for identifying Sudan Red Molecules Based on Raman Spectroscopy.* Trends in Applied Sciences Research, 2006. **1**: p. 155-161.